In Silico Discovery of Thioglycoside Analogues as Donor-Site Inhibitors of Glycosyltransferase LgtC

Olimpo Sierra-Hernandez

olimpos@uninorte.edu.co

Universidad del Norte

Oscar Saurith-Coronell

Universidad del Norte

Jackson J. Alcázar

Universidad del Desarrollo

Eliceo Cortés

instituto universitario de Barranquilla

Máryury C. Flores-Sumoza

Universidad Simón Bolívar

Juan D. Rodríguez-Macías

Universidad Libre

José R. Mora

Universidad San Francisco de Quito

Yovani Marrero-Ponce

Panamerican University

Ernesto Contreras-Torres

Universidad San Francisco de Quito

Article

Keywords: Thioglycoside analogues, Glycosyltransferase LgtC inhibition, In silico drug discovery, Antivirulence strategy, Gram-negative bacteria

Posted Date: December 17th, 2025

DOI: https://doi.org/10.21203/rs.3.rs-8233121/v1

Additional Declarations: No competing interests reported.

In Silico Discovery of Thioglycoside Analogues as Donor-Site Inhibitors of Glycosyltransferase LgtC

Olimpo Sierra-Hernández[1,2 +,*], Oscar Saurith-Coronell[1,2]; Jackson J. Alcázar[3], Eliceo Cortés[4], Maryury C. Flores-Sumoza[5]; Juan D. Rodríguez-Macías[6]; José R. Mora[7]; Yovani Marrero-Ponce[8,9], Ernesto Contreras-Torres[9,10] and Edgar A. Márquez Brazón[2*+].

[1] Departamento de Medicina, División Ciencias de la Salud, Universidad del Norte, Km 5, Vía Puerto Colombia, Puerto Colombia 081007, Colombia
[2] Grupo de Investigaciones en Química y Biología, Departamento de Química y Biología, Facultad de Ciencias Básicas, Universidad del Norte, Carrera 51B, Km 5, Vía Puerto Colombia, Barranquilla 081007, Colombia.
[3] Centro de Química Médica, Instituto de Ciencias e Innovación en Medicina, Facultad de Medicina, Clínica Alemana Universidad del Desarrollo, Santiago, Chile.
[4] Grupo de Investigación en Sociedad, Educación y Desarrollo HumanoGISEDH. Facultad de Ciencias, Educación, Artes y Humanidades. Institución Universitaria de Barranquilla 080002, Colombia.
5 Programa de Química y Farmacia, Facultad de Ciencias Básicas y Biomédicas, Universidad Simón Bolívar, Carrera 59 N° 59-65, Barranquilla 080002, Colombia.
6 Facultad de Ciencias de la Salud, Exactas y Naturales, Universidad Libre, Barranquilla 080001, Colombia
7 Grupo de Química Computacional y Teórica (QCT-USFQ), Departamento de Ingeniería Química, Universidad San Fr Facultad de Ingeniería, Universidad Panamericana, Augusto Rodin No. 498, Insurgentes Mixcoac, Benito Juárez, Ciudad de México 03920, Mexico
9 Grupo de Medicina Molecular y Traslacional (MeM&T), Colegio de Ciencias de la Salud (COCSA), Escuela de Medicina, Edificio de Especialidades Médicas, Diego de Robles y Vía Interoceánica, Universidad San Francisco de Quito (USFQ), Quito 170157, Ecuador.
10 Department of Organic and Inorganic Chemistry, Faculty of Science and Technology, University of the Basque Country (UPV/EHU), P.O. Box 644, 48940 Bilbao, Biscay, Spain.

Correspondence to: olimpos@uninorte.edu.co; ebrazon@uninorte.edu.co.
[+]these authors contributed equally to this work

ABSTRACT

The growing prevalence of multidrug-resistant Gram-negative pathogens highlights the urgent need for therapeutic strategies that complement traditional antibiotics by targeting essential virulence pathways. Glycosyltransferase LgtC, a key enzyme in lipooligosaccharide (LOS) biosynthesis, represents an attractive target for antivirulence approaches because of its essential role in bacterial immune evasion and pathogenicity. In this work, we employed an integrated *in silico* pipeline to identify thioglycoside analogs structurally related to the metabolic decoys FucSBn and BacSBn, evaluating their potential to hit the UDP-galactose donor pocket of LgtC. A similarity-based screening in PubChem, followed by ADME–Tox filtering yield 18 candidate analogs. Molecular docking using AutoDock-GPU revealed several candidates, most notably C-5 (−8.36 kcal/mol) and C-18 (−8.13 kcal/mol), to bind favorably within the donor site, showing more negative mean scoring values than natural donor UDP-α-D-galactose (−6.74 kcal/mol). Redocking of the natural ligand reproduced the crystallographic pose, supporting the reliability of the docking protocol. To assess dynamic behavior, 100 ns molecular dynamics simulations (AMBER14) were performed for each complex. The top-scoring analogs maintained stable binding poses, with RMSD values of ~2.0–3.0 Å and preserved donor-like hydrogen-bond networks complemented by π-stacking and sulfur-mediated contacts. These interaction patterns suggest that the thioglycoside analogs may occupy the donor site in a manner compatible with competitive binding. While docking and MD describe different aspects of ligand recognition, several trends observed in docking, such as the favorable binding scores of C-5 and C-18, are broadly consistent with their ability to maintain stable poses during MD. Based on this consistency and scoring, the thioglycoside scaffolds C-5, C-14, and C-18 emerge as computationally prioritized candidates for subsequent biochemical testing against LgtC. Furthermore, these scaffolds offer a mechanistic basis and putative

starting points for future structure-based optimization of thioglycoside analogs aimed at disrupting LOS biosynthesis in multidrug-resistant Gram-negative bacteria.

Keywords: *Thioglycoside analogues; Glycosyltransferase LgtC inhibition; In silico drug discovery; Antivirulence strategy; Gram-negative bacteria*

1. Introduction.

The global rise of multidrug-resistant (MDR) bacteria threatens to erode the effectiveness of existing antibiotics and compromising routine medical procedures.[1–4] This crisis is particularly acute for Gram-negative pathogens, where efficient resistance dissemination and the slow pace of antibiotic discovery have created a critical therapeutic gap.[5] The rapid spread of resistance is fueled by horizontal gene transfer and by environmental reservoirs continuously exposed to antibiotic residues, which together accelerate the emergence and persistence of MDR Gram-negative strains.[6–13]

Gram-negative pathogens such as *Neisseria spp., Haemophilus influenzae*, and members of the Enterobacteriaceae family combine low outer-membrane permeability, efflux pumps, and enzymatic antibiotic degradation, severely limiting the efficacy of conventional drugs.[14–19] This scenario has prompted the exploration of alternative strategies that do not rely solely on bactericidal activity but instead target key virulence pathways in these organisms.[20–23] In this context, *In silico* methodologies, including similarity-based screening, molecular docking, and molecular dynamics (MD) simulations, have become central to early-stage antibacterial discovery. These approaches enable the rapid prioritization of compounds with favorable binding and pharmacokinetic profiles, providing a cost-effective route to explore alternative targets and mechanisms of action in MDR Gram-negative bacteria.

Antivirulence strategies have emerged as a complementary approach to traditional antibiotics by targeting key pathogenic functions, such as toxin production, adhesion, or surface glycan remodeling, without directly compromising bacterial viability.[24,25] By attenuating virulence and facilitating immune clearance, these approaches can reduce the selective pressure for resistance development. In Gram-negative bacteria, surface glycoconjugates such as lipooligosaccharides (LOS) are central to immune evasion and serum resistance, making their biosynthetic enzymes attractive antivirulence targets.

For instance, biofilm formation is a major factor in the persistence and antibiotic resistance of Gram-negative pathogens. Biofilms act as physical and physiological barriers that limit antibiotic penetration and protect bacteria from immune clearance. Antivirulence therapies aimed at disrupting biofilm formation or promoting its dispersal have been shown to increase susceptibility to conventional antibiotics and improve eradication of chronic infections, particularly in medical device-related and pulmonary infections.[26] Likewise, inhibitors of the type III secretion system (T3SS), including small molecules that disrupt the formation of the injection needle or basal body assembly, can prevent the translocation of virulence effectors into host cells, thereby reducing tissue damage and inflammation. These approaches have been validated in models of *Salmonella*, *Yersinia*, *Shigella*, and *Pseudomonas*.[27] Additionally, well-characterized antivirulence targets such as LasR and PqsR in *Pseudomonas aeruginosa*, or EspA in enteropathogenic *E. coli*, have been identified as central regulators of multiple virulence traits and represent attractive candidates for rational drug design.[27] Furthermore, some antivirulence compounds have already demonstrated early clinical efficacy. CAL02, a lipid vesicle that sequesters pneumococcal toxins, and SAL200, a recombinant endolysin active against *Staphylococcus aureus*, have been evaluated in clinical trials and have shown promising safety and efficacy profiles.[26] Although most clinical advances have focused on Gram-positive pathogens, the same principles can be applied to Gram-negative bacteria, provided that challenges related to outer membrane permeability are addressed. While most antivirulence strategies under clinical or preclinical development target extracellular virulence factors, intracellular targets essential for glycan assembly offer an equally compelling therapeutic avenue.

Antivirulence strategies thus offer an alternative and complementary therapeutic approach to traditional antibiotic use, particularly in the context of multidrug-resistant Gram-negative pathogens. By targeting specific pathogenic functions without exerting lethal pressure, they help reduce the emergence of resistance while opening new avenues for the treatment of persistent and difficult-to-eradicate infections. Although formulation, pharmacokinetics, and clinical validation still require further development, antivirulence therapies stand as one of the most innovative and viable strategies in the current drug discovery landscape. Their synergy with conventional antibiotics may represent a critical step toward addressing the growing threat of resistance. Moreover, their reduced impact on the microbiota and potential applications in immunocompromised patients or as

adjuncts in chronic infections further underscore their therapeutic value.[25] However, even though antivirulence therapies reduce selective pressure, they remain non-bactericidal and therefore rely on host immunity for infection clearance.[28] This limitation underscores the need for well-defined molecular targets whose inhibition meaningfully attenuates virulence, such as LgtC, a key enzyme in LOS biosynthesis, while still allowing combination with conventional antibiotics when required.

Among the promising molecular targets in Gram-negative bacteria, glycosyltransferase LgtC has emerged as a key enzyme involved in the biosynthesis of lipooligosaccharides (LOS), which are critical for bacterial viability, immune evasion, and virulence. LgtC belongs to the CAZy GT-8 family and functions as a retaining glycosyltransferase, catalyzing the transfer of galactose residues to the LOS core in pathogens such as *Neisseria gonorrhoeae* and *Neisseria meningitidis*. Its structural characterization has revealed flexible regions and catalytic pockets amenable to inhibition, making it an attractive target for rational drug design.[29] Inhibiting LgtC disrupts LOS assembly, leading to truncated glycans and compromised bacterial surface architecture, which in turn attenuates virulence and sensitizes bacteria to host defenses. The LOS structure influences bacterial adhesion, immune evasion, serum resistance, and biofilm formation, all of which are key determinants of pathogenicity and transmission. Inhibiting LgtC disrupts the assembly of functional glycoconjugates, leading to truncated LOS structures that compromise membrane integrity and expose the bacteria to host immune defenses.

The relevance of LgtC as a target is further supported by thioglycoside "metabolic decoys" such as FucSBn and BacSBn (Figure 1), which mimic native donor substrates while incorporating sulfur linkages that resist enzymatic hydrolysis.[19] These compounds interfere with bacterial glycan biosynthesis and attenuate virulence, while showing minimal effects on key commensals such as *Bacteroides fragilis*. Notably, this selectivity contrasts with the related O-glycoside BnFucNAc, which disrupts CPS biosynthesis in *B. fragilis*, highlighting sulfur-linked glycomimetics as more selective scaffolds for antivirulence intervention.[19] Thus, thioglycosides constitute attractive starting points for the rational design of donor-site–targeted LgtC inhibitors.

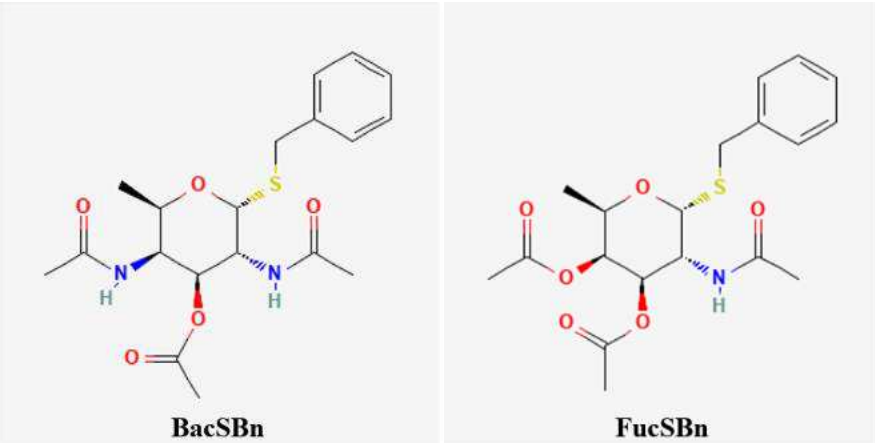

Figure 1. 2D structures for BacSBn and FucSBn, two thioglycosides reported as glycosyltransferase LgtC.

Despite the availability of structural information and the proof-of-concept metabolic decoys FucSBn and BacSBn, only a limited number of LgtC inhibitors have been reported, and in the best of our knowledge, no systematic study has explored thioglycosides as donor-mimetic ligands of the LgtC donor pocket using an integrated in silico workflow.[30] Therefore, In this study, we address this gap by implementing a similarity-based virtual screening pipeline centered on FucSBn and BacSBn, followed by ADME–Tox profiling, molecular docking, and 100 ns molecular dynamics simulations. Our aim is to identify thioglycoside analogs with favorable drug-like properties that stably occupy the UDP-galactose donor site of LgtC and thus act as putative competitive inhibitors of LOS biosynthesis. The resulting binding models provide a mechanistic basis and prioritized scaffolds for experimental validation and future structure-based optimization against multidrug-resistant Gram-negative pathogens.

2. Results and discussion.

2.1 Data collection.

Following the application of PubChem similarity criteria, a list of 18 candidate compounds was obtained. After evaluating these compounds using Lipinski's rules and the ADME-Tox protocol, it was confirmed that all of them met the necessary requirements for further analysis. These compounds are presented in Table 1, alongside FucSBn and BacSBn.

Table 1. ADME-Tox Evaluation and Comparative Analysis of Thioglycoside Analogs Targeting LgtC.

Compound	Iso-Smiles	Tox-Level	CID - Pubchem
FucSBn	C[C@@H]1[C@@H]([C@@H]([C@H]([C@H](O1)SCC2=CC=CC=C2)NC(=O)C)OC(=O)C)OC(=O)C	4	171378782
BacSBn	C[C@@H]1[C@@H]([C@@H]([C@H]([C@H](O1)SCC2=CC=CC=C2)NC(=O)C)OC(=O)C)NC(=O)C	4	171378781
C-1	CC(=O)N[C@H]1[C@H]([C@@H]([C@H](O[C@@H]1SC/C=C/C2=CC=CC=C2)COC(=O)C)OC(=O)C)OC(=O)C	4	70476062
C-2	CC(=O)NCC1C(C(C(C(O1)SC/C=C/C2=CC=CC=C2)O)O)O	4	20258414

C-3	CC(=O)N[C@@H]1[C@H]([C@@H]([C@H](O[C@H]1SCC2=CC=CC=C2)CO)O)O	4	46885357
C-4	CC1=CC=C(C=C1)S[C@H]2[C@@H]([C@H]([C@@H]([C@H](O2)COC(=O)C)OC(=O)C)OC(=O)C)NC(=O)C	4	52912941
C-5	CC(=O)N[C@H]1[C@H]([C@@H]([C@H](O[C@@H]1SCC=CC2=CC=CC=C2)COC(=O)C)OC(=O)C)OC(=O)C	4	54193385
C-6	CC(=O)N[C@H]1[C@H]([C@@H]([C@H](O[C@@H]1SCC=CC2=CC=CC=C2)CO)O)O	4	54294526
C-7	CC(=O)NC[C@@H]1[C@H]([C@@H]([C@@H]([C@H](O1)SCC=CC2=CC=CC=C2)O)O)O	4	54416964
C-8	CC(=O)N[C@@H]1[C@H]([C@@H]([C@H](O[C@@H]1SCC2=CC=CC=C2)CO)O)O	4	60155840

C-9	CC1=CC=C(C=C1)S[C@H]2[C@@H]([C@H]([C@H]([C@H](O2)COC(=O)C)OC(=O)C)OC(=O)C)NC(=O)C	4	66553249
C-10	CC(=O)N[C@H]1[C@H]([C@@H]([C@H](O[C@@H]1SC/C=C/C2=CC=CC=C2)COC(=O)C)OC(=O)C)OC(=O)C	4	70476062
C-11	CC(=O)N[C@@H]1[C@H]([C@@H]([C@H](O[C@H]1SC/C=C/C2=CC=CC=C2)CO)O)O	4	70476322
C-12	CC(=O)N[C@H]1[C@H]([C@@H]([C@H](O[C@@H]1SC/C=C/C2=CC=CC=C2)CO)O)O	4	70476320
C-13	CC(=O)NC[C@@H]1[C@H]([C@@H]([C@@H]([C@H](O1)SC/C=C/C2=CC=CC=C2)O)O)O	4	70477099
C-14	CC(=O)NC[C@@H]1[C@H]([C@@H]([C@@H]([C@@H](O1)SC/C=C/C2=CC=CC=C2)O)O)O	4	70477102

C-15	CO[C@@H]1CCOC[C@H]1NC(=O)CCSCC2=CC=CC=C2	5	91770848
C-16	CO[C@@H]1COCC[C@H]1NC(=O)CCSCC2=CC=CC=C2	5	91796185
C-17	CC(=O)NC1C(C(C(OC1SCC2=CC=CC=C2)COC(=O)C)OC(=O)C)OC(=O)C	4	137410510
C-18	CC(=O)N[C@@H]1[C@H]([C@@H]([C@H](O[C@H]1SCCC2=CC=CC=C2I)COC(=O)C)OC(=O)C)OC(=O)C	4	175198626

The ADME-Tox profiling of the selected thioglycoside analogs, including FucSBn and BacSBn, revealed favorable pharmacokinetic and safety characteristics (supporting material, table S1), supporting their potential as inhibitors of bacterial glycosyltransferase LgtC. All compounds were evaluated using *in silico* models, and their physicochemical properties were consistent with drug-likeness criteria, particularly Lipinski's Rule of Five. These parameters are essential for predicting oral bioavailability and systemic exposure, especially for intracellular targets such as LgtC. According to table S1, most compounds exhibited molecular weights between 309 and 479 Da, with only C-18 exceeding the 500 Da threshold. Despite this, C-18 maintained acceptable hydrogen bonding and lipophilicity values, suggesting it may still possess favorable pharmacokinetics. The hydrogen bond acceptors (HBA) ranged from 5 to 10, and donors (HBD) from 1 to 4, aligning with the optimal range for membrane permeability and solubility. For example, FucSBn and BacSBn showed 8 HBAs and 1–2 HBDs, while analogs such as C-5 and C-9 reached the upper limit of 10 HBAs but remained within acceptable bounds. On the other hand, LogP values which reflect lipophilicity ranged from 0.25 to 2.62, indicating moderate lipophilicity across the dataset. This is ideal for compounds targeting intracellular enzymes, as excessive lipophilicity can lead to poor solubility and off-target accumulation. FucSBn and BacSBn, with LogP values of 2.42 and 2.39 respectively, serve as benchmarks for optimal membrane permeability. Analog C-3, with a LogP of 0.25, is highly hydrophilic, which may favor solubility but limit passive diffusion. Conversely, C-15 and C-16, with LogP values of 2.62, are the most lipophilic, potentially enhancing membrane interaction but requiring careful monitoring for bioaccumulation.[30] However, it is important to highlight that the behavior of these compounds is also affected by porin selectivity and efflux susceptibility.[31–33] For this reason, determining these parameters may be necessary in future studies.

In terms of toxicity, most compounds were classified as Tox-Level 4, indicating moderate toxicity, while C-15 and C-16 were assigned Tox-Level 5, suggesting low toxicity. According to the Globally Harmonized System (GHS), Level 4 compounds may cause adverse effects at doses between 300–2000 mg/kg, whereas Level 5 compounds are considered safe at doses above 2000 mg/kg.[34] These findings suggest that the selected analogs could be used at low therapeutic doses without significant safety concerns.[35]

When compared to other reported inhibitors of LgtC, such as 5-methyl pyrazol-3-one derivatives, as well as the natural ligand, UDP-galactose analogs, the thioglycoside analogs in this study demonstrate comparable or superior ADME-Tox profiles. For instance, Ema et al. (2018) identified non-substrate-like inhibitors of LgtC with low micromolar activity but limited drug-likeness due to poor solubility and high molecular weight. In contrast, the analogs reported here maintain balanced polarity and lipophilicity, enhancing their potential for bioavailability and target engagement.[30] Moreover, the sulfur linkage in thioglycosides contributes to metabolic stability, as these bonds are less susceptible to enzymatic hydrolysis than O-glycosidic counterparts. This structural feature enhances the pharmacokinetic profile and supports their role as competitive inhibitors of glycosyltransferases. The analogs also mimic the structural and electronic features of natural substrates, increasing their likelihood of binding effectively to the catalytic pocket of LgtC.[30] These results confirm the suitability of all selected thioglycoside analogs for further computational and experimental investigation. Their physicochemical and safety profiles are consistent with known drug-like inhibitors of LgtC, and their structural diversity offers a valuable platform for exploring glycosyltransferase inhibition mechanisms.

2.2 Molecular docking.

2.3 Redocking protocols.

The redocking analysis shown in Figure 2 provides an essential validation of the computational approach used in this work. In the first panel, (left) the natural ligand UDP-α-D-galactose was successfully docked back into the catalytic pocket of LgtC, reproducing its crystallographic orientation with remarkable fidelity. The second panel (center) illustrates the positioning of the reference inhibitors FucSBn and BacSBn within the same active site. Both compounds occupy regions that overlap substantially with the natural ligand, suggesting that these analogs mimic the transition state of the enzymatic reaction and can effectively compete for the donor site. Finally, the third panel, which overlays all candidate ligands with UDP, demonstrates a consistent alignment across the dataset. This structural congruence indicates that the docking poses are not arbitrary but reflect a biologically plausible binding mode. The ability to reproduce the original crystal structure provides strong evidence of the reliability of the docking workflow, ensuring that the predicted interactions are meaningful.

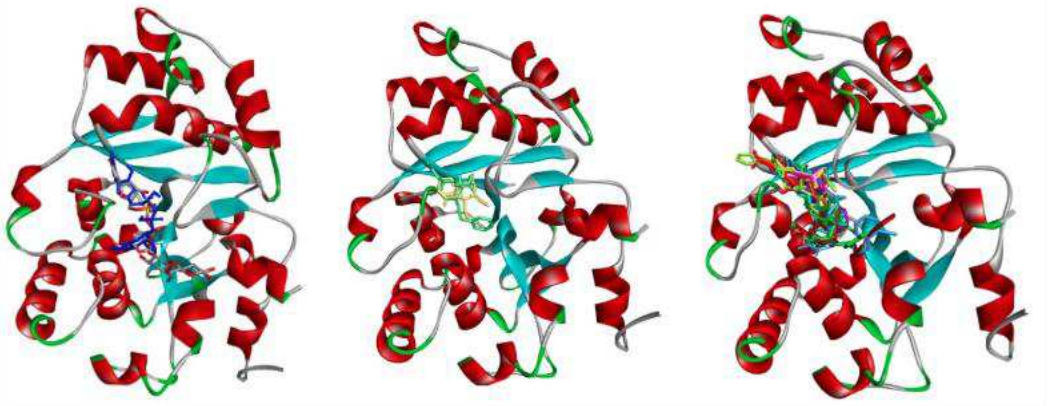

Figure 2. Validation of Docking Protocols Through Redocking: Natural Ligand and Thioglycoside Analogs in the LgtC Active Site. Left, natural ligands from pdb crystal superposed with the results in this work; center, FucSBn (yellow) and BacSBn (green) sugar into the active site; Right, all compounds studied here in superposing with the natural ligand.

2.4 Binding energies: scoring values

Several thioglycoside analogs demonstrated superior mean binding energies compared to UDP. C-5 (−8.36 kcal/mol) and C-18 (−8.13 kcal/mol) emerged as the strongest binders, outperforming the natural ligand by more than 1.5 kcal/mol on average. Other candidates, including C-14 (−7.84 kcal/mol) and C-13 (−7.77 kcal/mol), also exhibited favorable scores. Importantly, their standard deviations remained within acceptable ranges, indicating stable convergence across repeated runs rather than sporadic high affinity poses. Pose stability, reflected in RMSD values, further supports these findings. Most analogs maintained RMSD values comparable to or slightly above the natural ligand, suggesting that their binding orientations are consistent with the catalytic pocket geometry. BacSBn, while showing moderate affinity, displayed a slightly higher RMSD, which may indicate greater conformational variability during docking.

Among all candidates, C-5 and C-18 consistently outperformed the natural ligand UDP-α-D-galactose across 1,000 docking iterations, demonstrating not only superior mean binding energies (−8.36 and −8.13 kcal/mol, respectively) but also narrow standard deviations, indicative of stable convergence. This statistical robustness suggests that these compounds do not rely on sporadic high affinity poses but rather maintain a reproducible orientation within the catalytic pocket. When compared to UDP-α-D-galactose (−6.74 kcal/mol, SD 1.87), the improvement in affinity and consistency underscores their potential as lead inhibitors. These findings strengthen confidence in their suitability for downstream molecular dynamics simulations and rational optimization.

Table 2. Scoring values for both natural ligand and compounds study herein.

Mol-LgtC	Binding Energy (Kcal/mol)	Bind Energy Mean (Kcal/mol)	Standar deviation	RMSD
C-5	-8.36	-5.28	1.01	1.05
C-18	-8.13	-5.77	1.07	1.63
C-14	-7.84	-5.28	0.98	0.89
C-13	-7.77	-5.45	0.95	1.13
C-7	-7.69	-5.26	1.03	1.01
C-1	-7.61	-5.26	0.95	1.07
C-6	-7.55	-4.91	0.95	0.75
C-12	-7.49	-4.89	0.94	0.76
C-4	-7.36	-5.07	0.87	0.65
FucSBn	-7.29	-4.51	0.87	1.17
C-1	-7.23	-4.87	0.97	0.98
C-10	-7.14	-5.24	0.96	1.83
C-17	-7.03	-4.81	0.89	1.45
C-2	-6.94	-5.22	1.01	1.71
C-9	-6.92	-4.99	0.85	1.55
UDP-α-D-galactose	-6.74	-1.53	1.87	1.77
C-16	-6.59	-5.33	0.75	1.11
C-8	-6.59	-4.60	0.95	0.81
C-15	-6.42	-5.21	0.77	1.19
C-3	-6.40	-4.57	0.96	1.95
1	-5.72	-4.70	0.92	1.98

2.5 Molecular Interactions into the active site.

To be more inside about the possible molecular interactions between ligands and proteins, a 2D diagram of interaction was generated. Figure 3 shows the molecular interaction not only for the natural ligands-generated from crystal pdb structure- but also for all compounds of study herein. According to figure 3, the natural ligand UDP-α-D-galactose establishes a canonical interaction network within the catalytic pocket of glycosyltransferase LgtC, essential for its role in lipooligosaccharide biosynthesis. Its interaction profile includes conventional hydrogen bonds (pink) anchoring the uracil, ribose, and phosphate groups to catalytic residues; carbon–hydrogen interactions (orange) stabilizing the ribose and pyrophosphate region; van der Waals contacts (green) ensuring steric complementarity; and π-stacking interactions (red) between the uracil ring and aromatic side chains. This pattern mirrors the crystallographic pose reported for LgtC and supports productive donor binding during galactose transfer.[36]

In contrast, the thioglycoside analogs (e.g., C-5 or C-18) retain the core hydrogen bond network (green) required for anchoring

but redistributes non-covalent contributions toward hydrophobic and aromatic contacts. Notably, it introduces π-alkyl interactions (purple) with aliphatic side chains and π-sulfur interactions (yellow) associated with the thioglycosidic linkage, alongside extensive van der Waals contacts (green) over the aromatic aglycone. These features, absent in UDP-α-D-galactose, explain the enhanced affinity of certain analogs and their ability to act as competitive inhibitors by mimicking aspects of the transition state while exploiting hydrophobic subpockets.[19,20,30]

Superposition of UDP-α-D-galactose with these analogs reveals spatial congruence in the donor region: the sugar moiety and glycosidic linkage of the analog align with the catalytic trajectory, while the aromatic aglycone explores lateral cavities not occupied by UDP-α-D-galactose. This local plasticity enables energy gain through π-stacking, and π-alkyl interactions without sacrificing essential hydrogen bonds. Consequently, analogs compensate for the absence of phosphate groups, critical in UDP-α-D-galactose for electrostatic interactions, by forming hydrophobic and π-sulfur (yellow) contacts that stabilize the complex.[37]

So far, the combination of (i) validation by redocking, (ii) coherent superposition of analogs over donor determinants, and (iii) statistical robustness from 1,000 runs confirms that these poses are reliable starting points for molecular dynamics simulations. Such simulations will assess the persistence of hydrogen bonds, quantify contributions from π-stacking and π-alkyl, and evaluate the stability of π-sulfur contacts under near-physiological conditions.[38] On the other hand, due to a small difference in the scoring value for natural ligands, all compounds were taken to the molecular dynamics protocol.

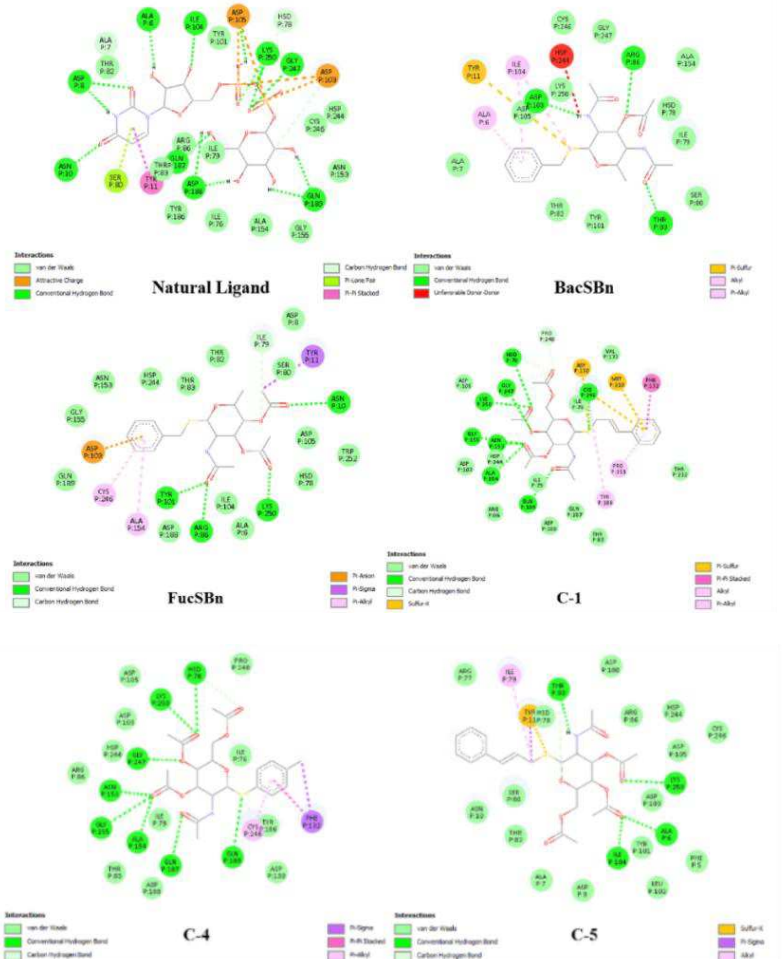

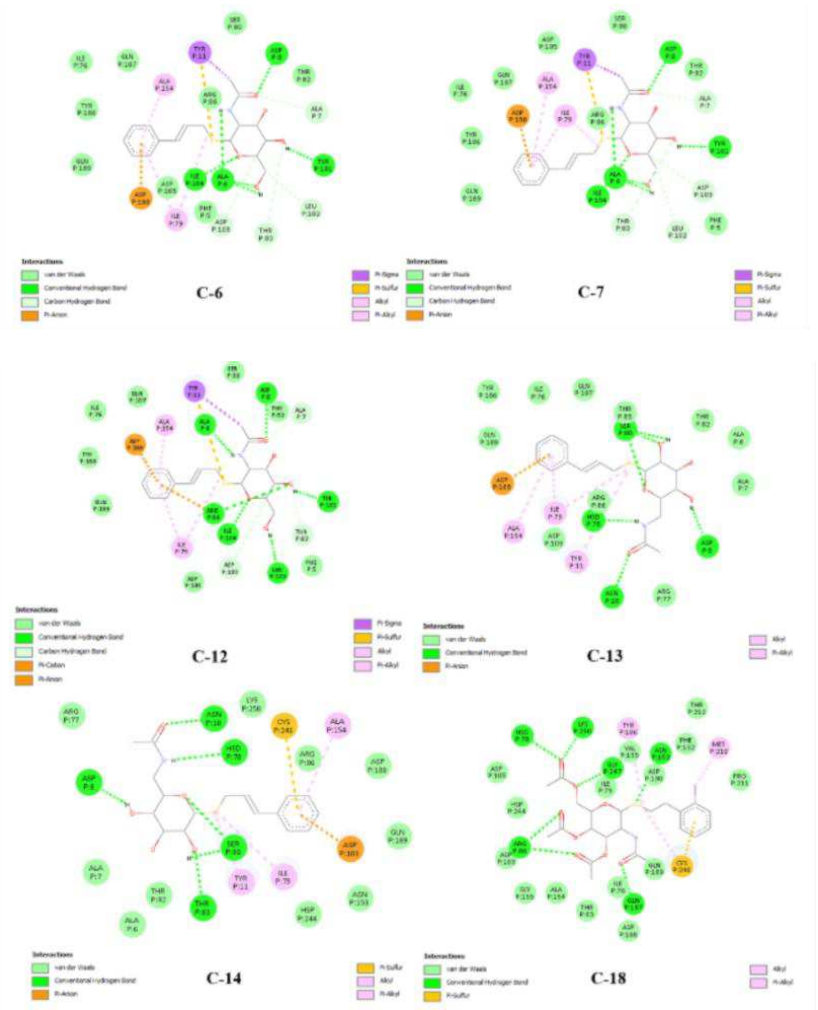

Figure 3. Interaction of fingerprints of the natural ligand and thioglycoside analogs within the LgtC active site.

2.6 Molecular Dynamics: Structural analysis.

The RMSD profiles across all simulated systems provide insight into the structural stability of LgtC–ligand complexes during the 100 ns molecular dynamics runs. The first set of graphs (UDP-α-D-galactose, BacSBn, FucSBn, and C-1) shows that the natural ligand UDP maintained the lowest RMSD values, fluctuating between 1.0 and 2.5 Å after an initial equilibration phase (~10–20 ns), confirming its native compatibility with the catalytic pocket. BacSBn exhibited a similar trend, stabilizing near 2.5 Å, while FucSBn and C-1 reached slightly higher deviations (~3.0 Å), reflecting minor conformational adjustments to optimize hydrophobic and sulfur-mediated contacts. The second set of graphs (C-4, C-5, C-6, C-7, C-12, C-13, C-14, and C-18) highlights the behavior of top-scoring analogs identified during docking. Most analogs stabilized after 20 ns, with RMSD values ranging from 2.0 to 3.0 Å. Notably, C-5 and C-18, previously identified as high-affinity ligands, displayed consistent stability throughout the trajectory, maintaining RMSD values comparable to or slightly above UDP. The subtle dynamic fluctuations observed provide valuable information for optimizing their interaction profile Other analogs, such as C-13 and C-14, showed transient fluctuations before convergence, suggesting local rearrangements without compromising overall complex integrity. Conversely, the RMSD analysis complements the docking results by confirming that high-affinity ligands identified in silico also exhibit dynamic stability within the LgtC active site. The natural ligand (UDP-α-D-galactose), which served as the baseline, maintained the lowest RMSD values (<2.5 Å), consistent with its physiological role and moderate docking score (−6.74 kcal/mol). Thioglycoside analogs such as C-5 and C-18, which achieved the most favorable docking energies (−8.36 and −8.13 kcal/mol, respectively),

displayed RMSD profiles comparable to UDP after equilibration, indicating strong pocket accommodation and minimal structural drift. Conversely, ligands with intermediate docking scores (e.g., C-13, C-14) exhibited transient RMSD fluctuations before stabilization, suggesting local rearrangements to optimize hydrophobic and sulfur-mediated contacts. This agreement between docking affinity and dynamic stability reinforces the reliability of the computational pipeline, indicating that C-5 and C-18 merit further consideration for experimental testing and their optimization. The RMSD profiles across all simulated systems provide insight into the structural stability of LgtC–ligand complexes during the 100 ns molecular dynamics (MD) runs. Notably, natural ligand, maintained RMSD values between 1.0 and 2.5 Å after an initial equilibration phase (~10–20 ns), confirming its native compatibility with the catalytic pocket. This is consistent with reports that successful redocking of nucleotide sugars typically achieves RMSD < 2.0–2.5 Å when reproducing crystallographic poses.[39] The docking score for UDP (−6.74 kcal/mol) also falls within the expected range for native donors in GT active sites, as documented in GTDB-based workflows using AutoDock Vina.[40]

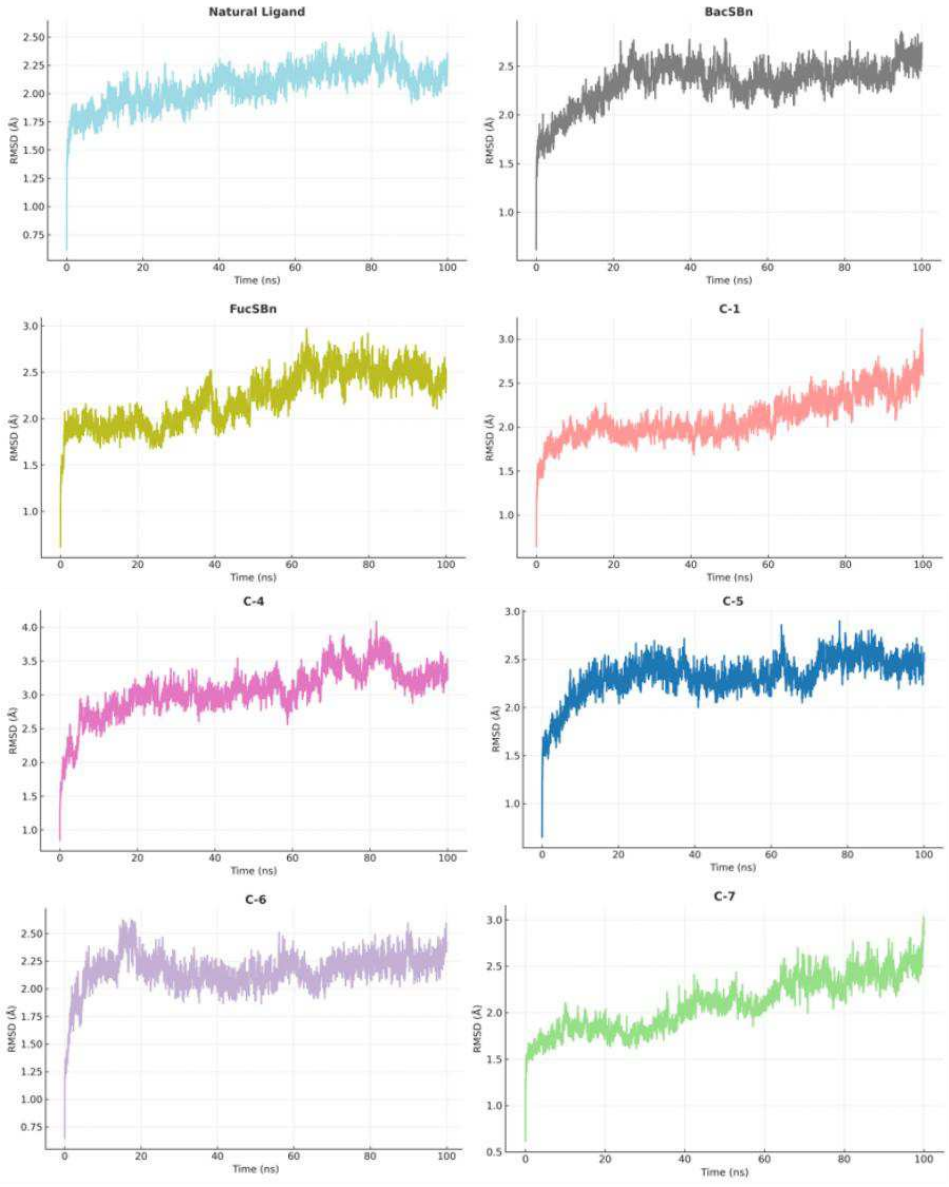

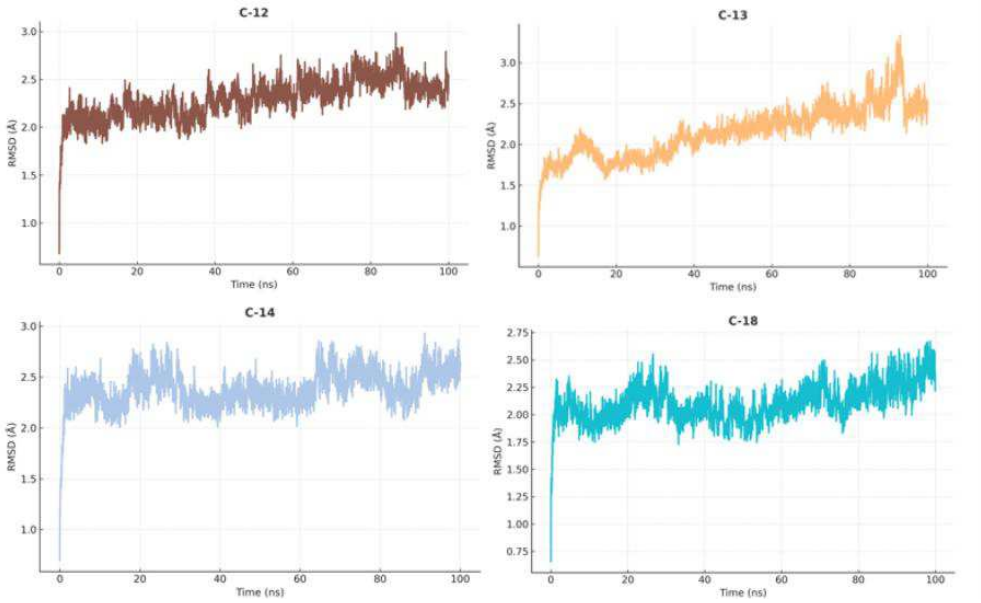

Figure 4. Molecular Dynamics RMSD Profiles of UDP-α-D-galactose and Thioglycoside Analogs in LgtC.

2.7 Molecular Dynamics: Radius of gyration.

The radius of gyration (Rg) is a structural parameter that quantifies the compactness of a molecular system. In molecular dynamics (MD) simulations, Rg is commonly used to assess the global stability and folding behavior of proteins and their complexes with ligands.[41] In antibiotic research, Rg is used to evaluate how potential inhibitors affect the structural compactness of bacterial target proteins. A stable or reduced Rg after ligand binding suggests that the compound may stabilize the protein, which is often desirable for effective inhibition.[42,43]

In this line, the Rg values were analysis for the compounds study herein using UDP-α-D-galactose and FucSBn and BacSBn as comparative indicators. According to the figure, the Rg profile of UDP-α-D-galactose, remained consistently within the range of 18.4–18.6 Å throughout the 100 ns simulation. This narrow fluctuation window reflects a highly stable and compact binding mode, consistent with its evolutionary optimization for the LgtC active site. Such behavior aligns with literature benchmarks, where stable protein–ligand complexes typically exhibit Rg values between 18.0–19.0 Å for similarly sized systems.[44] Several analogs, including C-5, C-14, and C-18, closely mirrored UDP's Rg behavior, maintaining values between 18.4 and 18.7 Å with minimal deviation These compounds integrate into the binding pocket without inducing substantial changes in protein compactness, indicating that their binding does not destabilize the overall protein structure. Their structural compatibility with LgtC supports their candidacy as potential inhibitors with favorable dynamic profiles.

In contrast, BacSBn and FucSBn, both previously reported as glycosyltransferase inhibitors, displayed more pronounced Rg fluctuations, occasionally exceeding 19.0 Å. This behavior suggests that their binding may induce local rearrangements or increased flexibility within the protein structure. While such dynamics could be interpreted as destabilizing, they may also reflect an alternative inhibitory mechanism, such as allosteric modulation or aglycone-driven conformational adaptation. Importantly, despite their higher Rg variability, both BacSBn and FucSBn remained stably associated with LgtC throughout the simulation, reinforcing their functional relevance as inhibitors. Other analogs, such as C-13 and C-7, showed intermediate Rg profiles, with values ranging from 18.5 to 19.0 Å. These compounds may require modest structural accommodation within the active site, which could influence their binding kinetics or specificity. Meanwhile, ligands such as C-1, C-6, C-12, and C-4 presented moderate fluctuations, suggesting a balance between affinity and flexibility.

Taken together, the Rg analysis complements RMSD and docking data, offering a multidimensional view of ligand-induced structural dynamics. The analogs C-5, C-14, and C-18 stand out for their ability to maintain compact and stable complexes, closely resembling the behavior of UDP-α-D-galactose. BacSBn and FucSBn, despite their higher Rg variability, remain relevant due to their reported inhibitory activity and sustained binding, highlighting the diversity of mechanisms by which glycosyltransferase inhibition may be achieved.

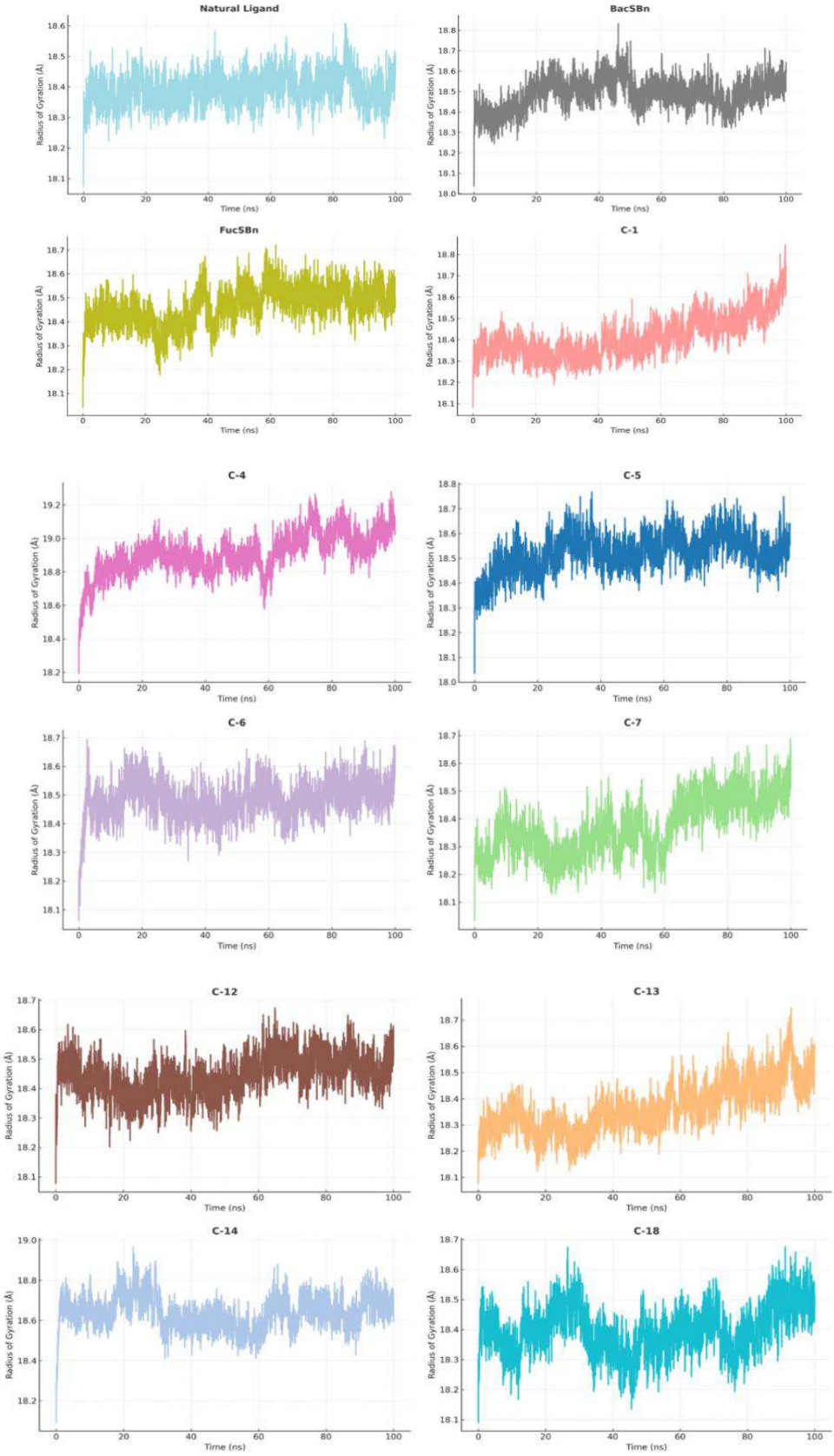

Figure 5. Radius of gyrations for all compounds of study in this work, at 100 ns.

2.8 Molecular Dynamics analysis: Root Mean Square Fluctuation (RMSF).

Root Mean Square Fluctuation (RMSF) is a key parameter in molecular dynamics (MD) simulations that quantifies the flexibility of individual residues within a protein over time. Unlike RMSD, which provides a global measure of structural deviation, RMSF offers a residue-level perspective, highlighting regions of the protein that undergo significant motion or remain rigid during ligand binding.[45,46]

In the context of antibiotic design, RMSF is particularly valuable for identifying functionally relevant dynamics in bacterial enzymes. Regions with low RMSF values often correspond to structurally conserved or catalytically essential residues, while elevated RMSF may indicate allosteric sites, loop regions, or binding-induced conformational changes. Understanding these fluctuations helps researchers pinpoint where and how a ligand exerts its effect, whether stabilizing the active site or disrupting flexible domains critical for function; on the other hand, in the context of glycosyltransferase LgtC, RMSF is particularly informative for identifying regions of structural rigidity and dynamic adaptation, both of which are critical for understanding ligand engagement and inhibitory potential.

According to the figure 6, across all ligand-bound simulations, the RMSF profiles reveal a consistent pattern: most residues exhibit low to moderate fluctuations (below 2.0 Å), indicating that the overall protein structure remains stable regardless of the ligand bound. This baseline stability is especially evident in the complex with UDP, the natural ligand, which shows minimal deviation across the entire residue index. Such behavior is consistent with literature reports, where native substrates typically induce minimal residue-level perturbations in their target enzymes.[47]

Two distinct regions, residues 0–50 and 200–250, consistently exhibited the lowest RMSF values across all ligand-bound systems. These segments represent interaction hotspots, likely encompassing key residues within the catalytic pocket and adjacent stabilizing domains. Their persistent rigidity suggests strong and sustained interactions with the ligands, reinforcing their functional importance in substrate recognition and enzymatic activity. This interpretation is strongly supported by the 2D docking interaction diagrams, which show that most hydrogen bonds, Van der Waals contacts, and π-interactions occur within these same residue ranges. For instance, in the UDP-α-D-galactose complex, critical interactions are concentrated in the N-terminal region and central binding pocket, precisely where RMSF values are lowest. Similarly, analogs such as C-5, C-14, and C-18 hit in these stable regions, mirroring UDP's dynamic footprint and reinforcing their potential as rationally designed inhibitors. In contrast, BacSBn and FucSBn, exhibited elevated RMSF values in loop regions outside the core interaction zones, with fluctuations occasionally exceeding 3.0 Å. These peaks were localized and may correspond to structural rearrangements required to accommodate their bulkier aglycone moieties. While such flexibility might suggest destabilization, it may also represent an adaptive binding mechanism, particularly relevant for inhibitors that function via induced fit or allosteric modulation. Importantly, despite these localized fluctuations, the overall structural integrity of LgtC remained intact, and ligand binding was sustained throughout the simulation. This dynamic behavior is consistent with findings from high-throughput MD workflows that assess ligand-induced flexibility as a predictor of binding mode diversity and potency.[48] Other analogs, such as C-13, C-7, and C-6, showed intermediate RMSF profiles, with modest increases in flexibility across peripheral regions. These compounds may require structural optimization to reduce unnecessary dynamics while preserving effective engagement with the core binding residues.

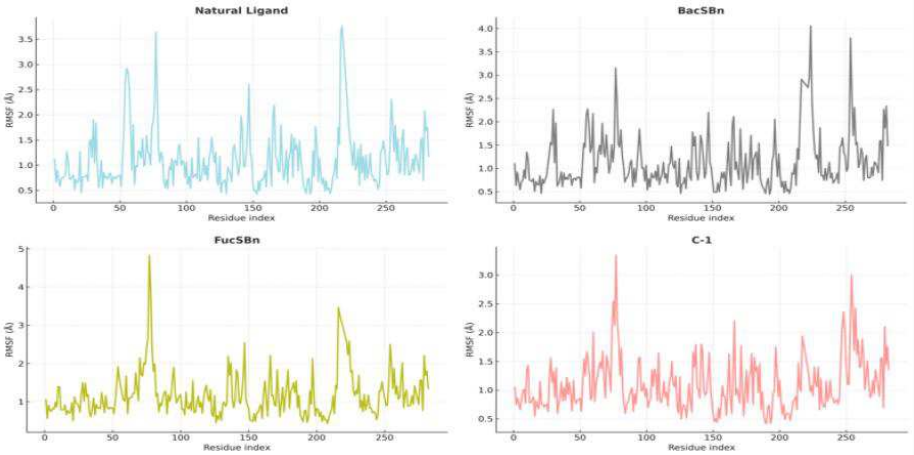

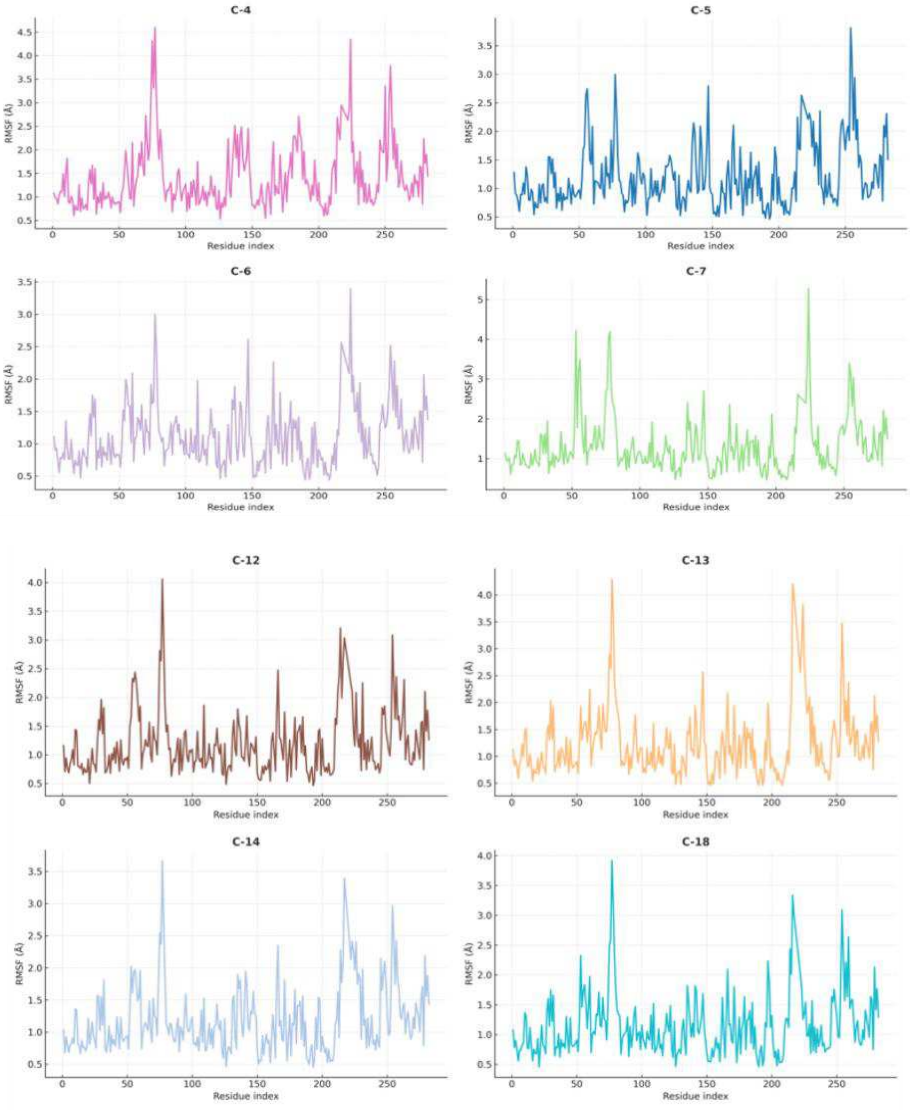

Figure 6. Residue-Level Flexibility of LgtC–Ligand Complexes: RMSF Profiles and Interaction Hotspots.

2.9 Molecular Dynamics: Binding Energy Analysis.

In molecular dynamics-based drug discovery, the binding energy of a ligand–protein complex is a critical parameter that reflects the thermodynamic favorability of the interaction. It integrates contributions from Van der Waals forces, electrostatic interactions, solvation effects, and entropic penalties. These components collectively determine how tightly and stably a ligand binds to its target, an essential criterion for antibiotic efficacy.[49] It is important to point out that in Yasara software convention, more positive values represent a more stable interaction.

Figure 7 shows the Binding energy trayectory. The natural ligand UDP, serving as the positive control, exhibited a consistently stable binding energy profile, with minimal fluctuations and an average value around −46 kcal/mol. This stability aligns with its evolutionary optimization for the LgtC active site and reinforces its role as a benchmark for evaluating analog performance. Its behavior is consistent with literature-reported binding energies for nucleotide-sugar donors in glycosyltransferase systems.[50]

According to figure 7, BacSBn and FucSBn, displayed more pronounced fluctuations in their binding energy profiles. Despite this variability, their average binding energies remained comparable to UDP-α-D-galactose, suggesting that these compounds

maintain strong interactions with the protein, albeit through potentially more dynamic or adaptive binding modes. This behavior may reflect the influence of their bulkier aglycone moieties, which could induce local rearrangements or engage in non-canonical contacts within the binding pocket. Such flexibility, while distinct from UDP's rigid approach, does not necessarily compromise inhibitory potential and may even support alternative mechanisms of action, such as allosteric modulation or induced fit.

When compared to the broader set of analogs (C-1 through C-18), several compounds, particularly C-5, C-14, and C-18, demonstrated binding energy profiles that closely mirror UDP-α-D-galactose, both in terms of average values and stability over time. These analogs maintained consistent interaction strength and minimal energetic drift, reinforcing their candidacy as rationally designed inhibitors. Their performance suggests a high degree of structural compatibility with the LgtC active site and supports the findings from RMSD, RMSF, and Rg analyses. Other analogs, such as C-1, C-13, and C-7, showed greater variability in binding energy, with trends indicating either gradual destabilization or transient interaction phases. While these compounds may still engage the protein effectively, their dynamic profiles suggest a need for further optimization to enhance binding persistence and reduce entropic penalties.

According to these results, C-5, C-14, and C-18 emerge as the top computationally ranked analogs, combining favorable energy with dynamic stability under simulated conditions. Meanwhile, BacSBn and FucSBn, despite their fluctuating profiles, remain relevant due to their sustained average binding energies and previously validated inhibitory activity.[51]

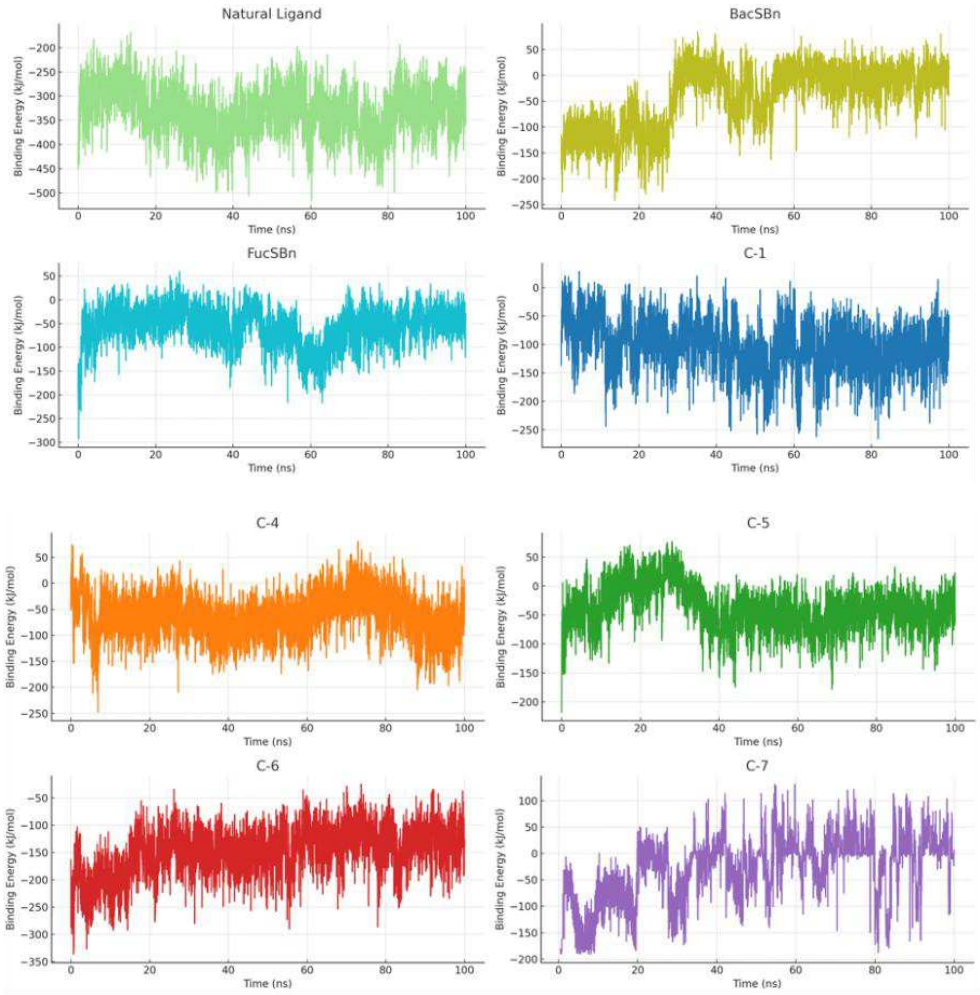

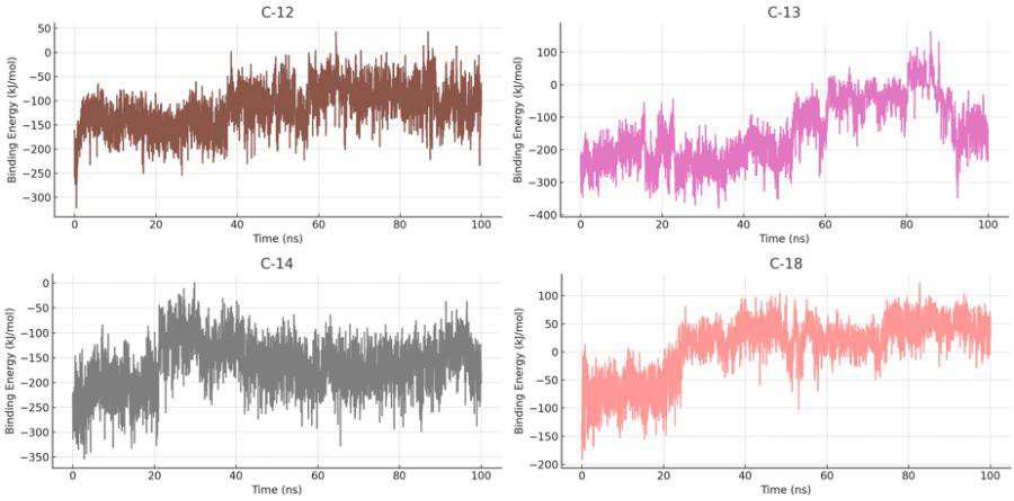

Figure 7. Binding Energy Profiles of LgtC–Ligand Complexes During 100 ns MD Simulations.

Following the analysis of the binding energy trajectories, we evaluated the mean binding energies for all ligand–protein complexes. To gain a more comprehensive understanding of the interaction profiles, solvation energy and potential energy were also compared across the different systems. These parameters collectively provide insight into the stability and thermodynamic favorability of ligand binding. For reference, the natural ligand was included as a positive control, enabling a direct comparison between the tested compounds and the native interaction. The results are summarized in table 3 below.

Table 3. Average ligand binding energy, change in potential, and solvation energy for complexes between compounds and LgtC.

Complex Compund-LgtC	Binding Energy (kcal/mol)	ΔE Potential (kcal/mol)	ΔE Solvation (kcal/mol)
UDP-α-D-galactose	-79.20	133.81	-213.01
BacSBn	-8.71	52.33	-61.04
FucSBn	-12.97	49.56	-62.54
1	-24.94	79.01	-103.95
4	-15.26	95.20	-110.47
5	-8.79	39.07	-47.86
6	-34.69	59.94	-94.63
7	-4.89	17.98	-22.87
12	-26.91	49.06	-75.96
13	-33.50	45.00	-78.50
14	-38.80	63.33	-102.13
18	3.33	35.63	-32.30

According to Table 3, UDP-α-D-galactose, the natural ligand, displayed the lowest binding energy value (−79.2 kcal/mol), corresponding to the strongest interaction in the YASARA/AMBER14 MM/PBSA evaluation. In contrast, several synthetic ligands achieved more positive binding energies; therefore, according to YASARA convention, suggesting a higher likelihood of forming stable complexes with LgtC. Notably, compound 18 exhibited the most positive value (+3.33 kcal/mol), followed by compounds such as 5 (−8.79 kcal/mol) and 7 (−4.89 kcal/mol), which also scored better than the natural ligand under this interpretation. Besides, the computational observations for BacSBn and FucSBn, both previously reported glycosyltransferase inhibitors, agree with experimental findings. Enzymatic assays have confirmed that compounds with similar structural features effectively reduce glycosyltransferase activity, validating their inhibitory potential.[52] These inhibitors often exhibit non-

classical binding behaviors, including induced fit and allosteric modulation, which can lead to structural flexibility without compromising potency.[53] This aligns with our MD results, where BacSBn and FucSBn maintained strong average binding energies and stable interactions in key catalytic regions, despite localized RMSF peaks and Rg variability. Furthermore, reviews on glycosyltransferase-targeted drug design confirm that inhibitors achieving binding energies comparable to or slightly better than natural substrates often translate into biologically relevant activity, even when structural adaptation occurs during binding.[54] This reinforces the interpretation that BacSBn and FucSBn, despite their dynamic profiles, remain promising candidates for antibiotic development. Interesting, comparing MD-derived descriptors (RMSD, Rg, and RMSF) with docking results, suggesting that they are supporting each other: ligands with positive or moderately negative binding energies (e.g., compounds 18, 5, and 7) maintained lower RMSD fluctuations and stable Rg values, indicating that these complexes remained structurally compact throughout the simulation.

Energy decomposition provides additional insight. For compounds with positive binding energies, the potential energy contribution was moderate, but the solvation term was less unfavorable compared to the natural ligand, which exhibited a highly negative solvation energy (−213.01 kcal/mol). This suggests that desolvation penalties significantly impact the natural ligand's overall stability in the simulated environment, whereas synthetic compounds may achieve a better balance between desolvation and interaction energy. These results indicate that, under YASARA's scoring interpretation, several synthetic ligands, particularly compound 18, could represent promising candidates for further optimization. Their favorable binding energies, combined with stable MD profiles, suggest a strong potential for effective interaction with LgtC.

2.10 Molecular Dynamics: The molecular interactions in the equilibrium.

Understanding the molecular interactions that persist during equilibrium is essential for validating the stability and functional relevance of ligand–protein complexes. While docking provides a static snapshot of binding, molecular dynamics (MD) simulations reveal how these interactions evolve under near-physiological conditions, accounting for flexibility, solvation, and entropic effects. At equilibrium, the focus shifts from transient contacts to persistent interaction networks, hydrogen bonds, hydrophobic contacts, π-stacking, and electrostatic bridges, that collectively stabilize the complex. Analyzing these patterns allows us to identify which residues act as anchoring points, how ligands adapt to the catalytic pocket, and whether induced-fit mechanisms contribute to binding. This dynamic perspective is critical for distinguishing strong, reproducible interactions from those that are merely artifacts of initial docking, ultimately guiding the rational optimization of lead compounds. Figure 8 shows the 2D molecular interactions diagrams for ligands-protein study in this work at 50 ns, generated by means of Discovery Study Visualizer.

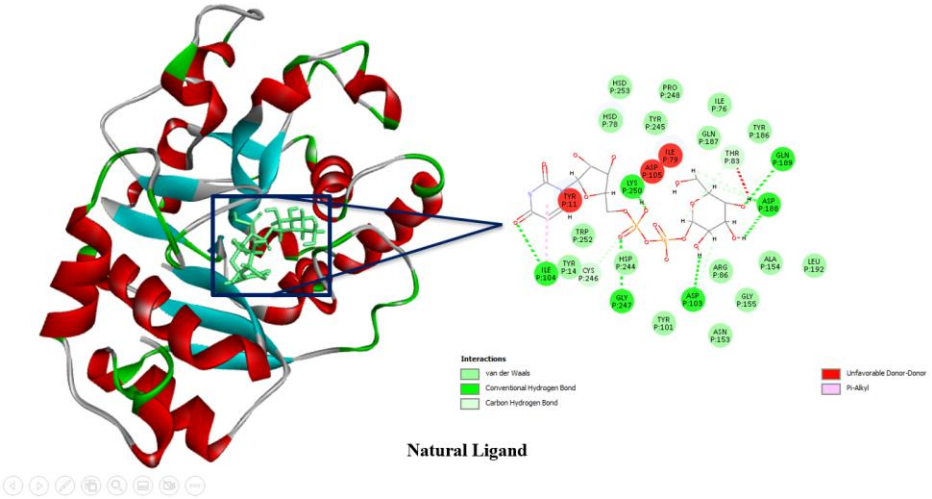

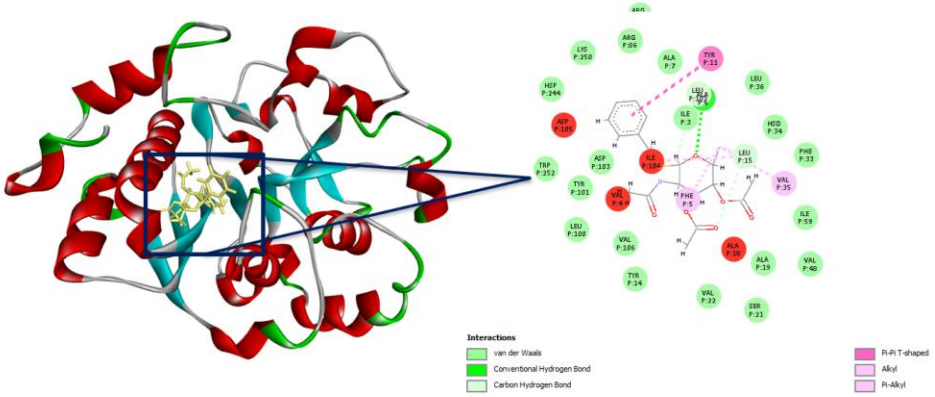

FucSBn

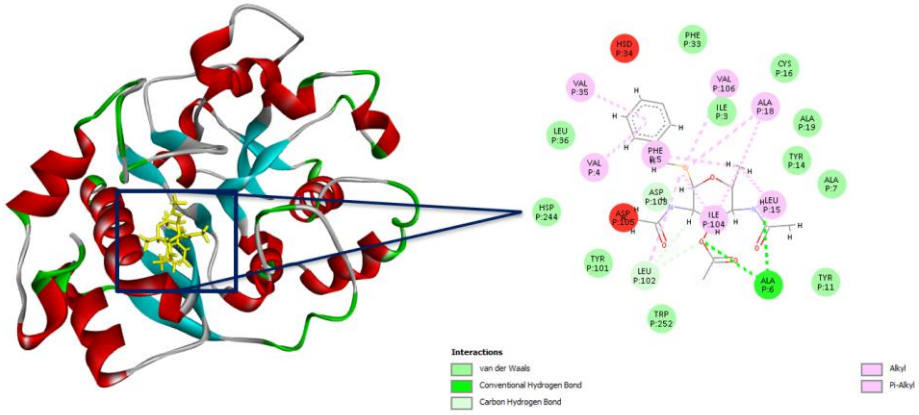

BacSbn

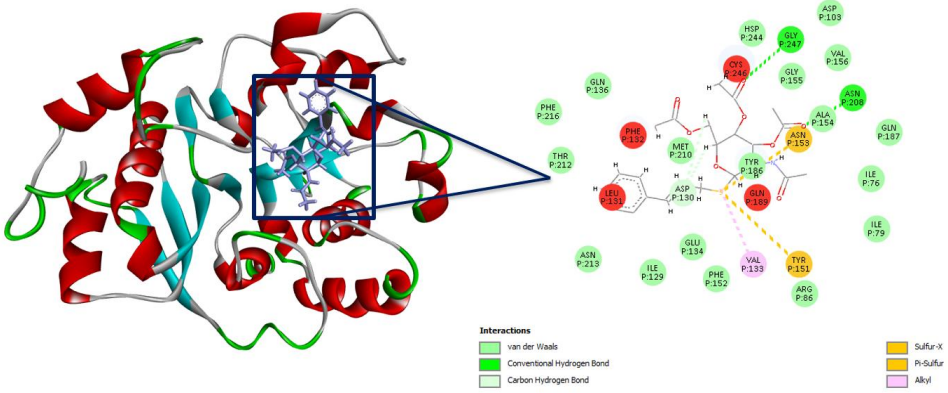

C-1

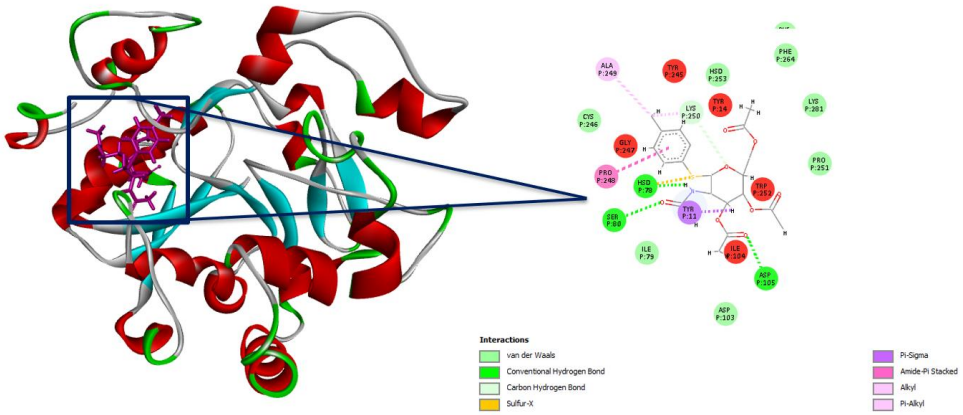
Interactions
van der Waals
Conventional Hydrogen Bond
Carbon Hydrogen Bond
Sulfur-X
Pi-Sigma
Amide-Pi Stacked
Alkyl
Pi-Alkyl

C-4

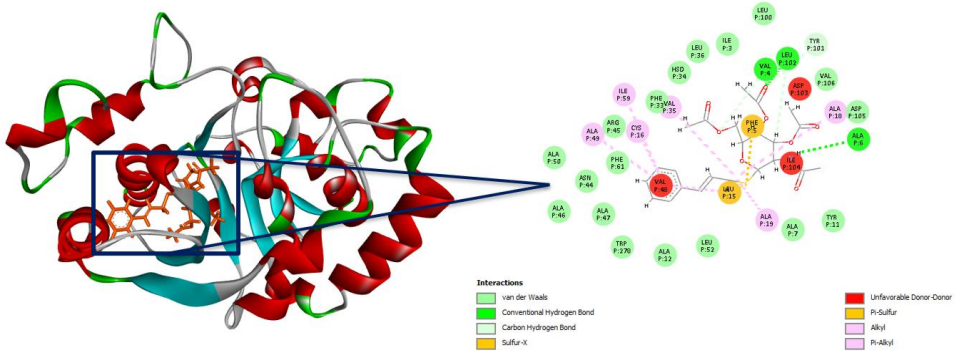
Interactions
van der Waals
Conventional Hydrogen Bond
Carbon Hydrogen Bond
Sulfur-X
Unfavorable Donor-Donor
Pi-Sulfur
Alkyl
Pi-Alkyl

C-5

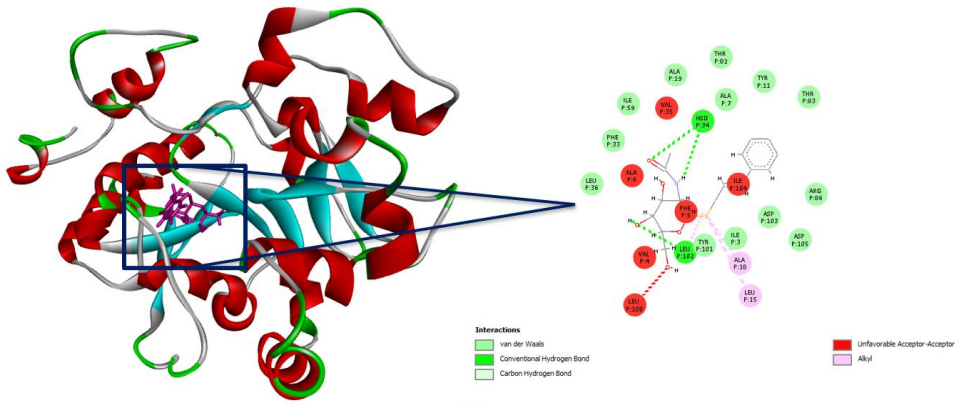
Interactions
van der Waals
Conventional Hydrogen Bond
Carbon Hydrogen Bond
Unfavorable Acceptor-Acceptor
Alkyl

C-6

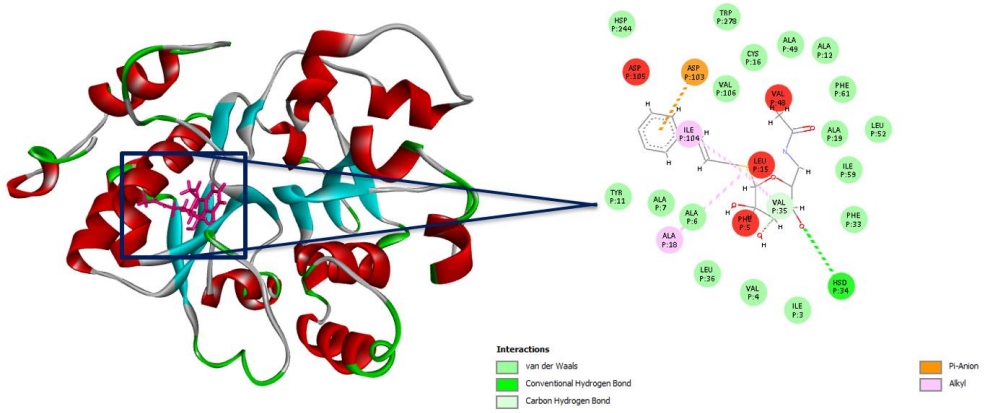
HSP P:244
TRP P:278
ASP P:105
ASP P:103
CYS P:16
ALA P:49
ALA P:12
VAL P:106
VAL P:48
PHE P:61
ILE P:104
ALA P:19
LEU P:52
LEU P:15
ILE P:59
TYR P:11
ALA P:7
ALA P:6
VAL P:35
PHE P:5
PHE P:33
ALA P:18
LEU P:36
HSD P:34
VAL P:4
ILE P:3
Interactions
van der Waals
Conventional Hydrogen Bond
Carbon Hydrogen Bond
Pi-Anion
Alkyl

C-7

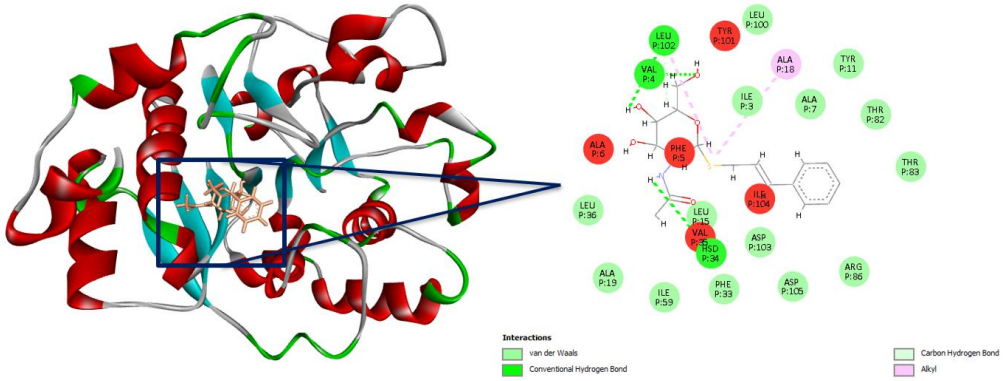
LEU P:100
LEU P:102
TYR P:101
VAL P:4
ALA P:18
TYR P:11
ILE P:3
ALA P:7
THR P:82
ALA P:6
PHE P:5
THR P:83
LEU P:36
ILE P:104
LEU P:15
VAL P:35
ASP P:103
HSD P:34
ARG P:86
ALA P:19
PHE P:33
ASP P:105
ILE P:59
Interactions
van der Waals
Conventional Hydrogen Bond
Carbon Hydrogen Bond
Alkyl

C-12

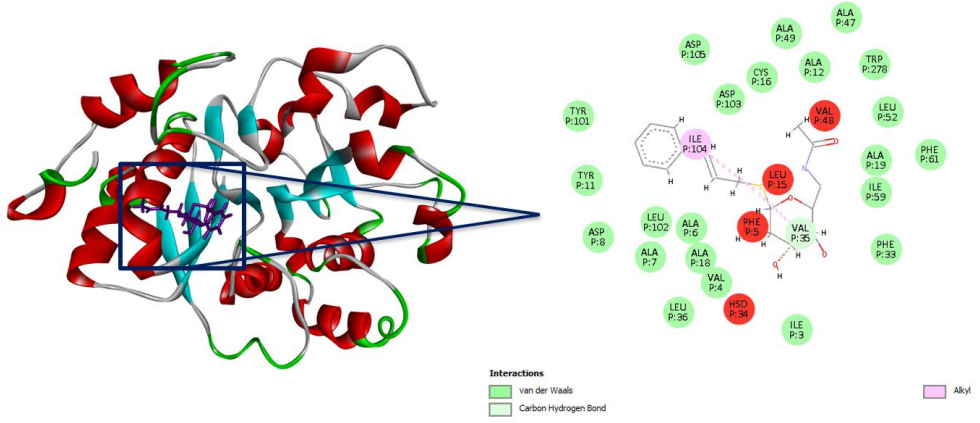
ALA P:47
ALA P:49
ASP P:105
ALA P:12
TRP P:278
CYS P:16
ASP P:103
TYR P:101
VAL P:48
LEU P:52
ILE P:104
PHE P:61
TYR P:11
LEU P:15
ALA P:19
ILE P:59
LEU P:102
ALA P:6
PHE P:5
VAL P:35
ASP P:8
ALA P:7
ALA P:18
PHE P:33
VAL P:4
LEU P:36
HSD P:34
ILE P:3
Interactions
van der Waals
Carbon Hydrogen Bond
Alkyl

C-13

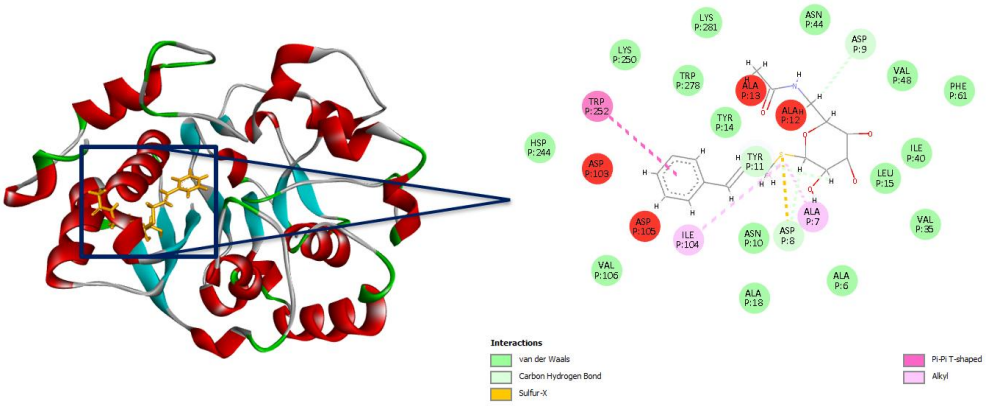

C-14

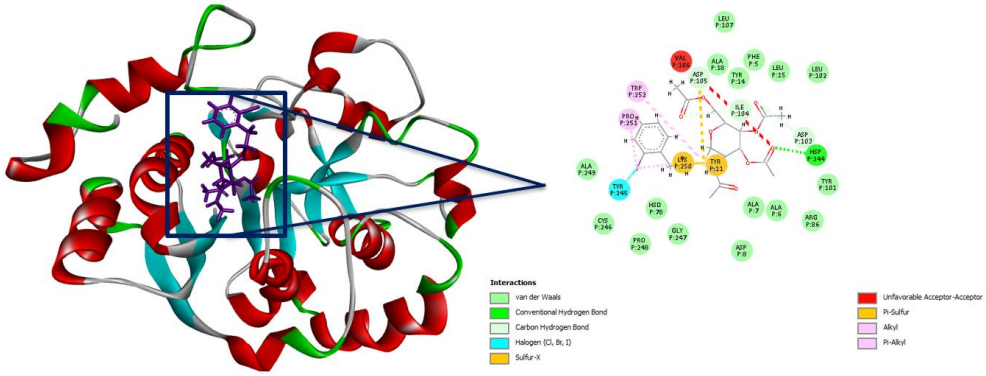

C-18

Figure 8. 2D molecular interaction diagram for equilibrium complexes from molecular Dynamics.

At equilibrium, molecular dynamics simulations revealed that all ligand–LgtC complexes reorganized into persistent interaction networks that differ subtly from the static docking poses. The natural ligand UDP-α-D-galactose maintained its canonical phosphate-anchored hydrogen-bond spine, complemented by π-stacking with aromatic residues near the uracil moiety. This profile mirrors the crystallographic pose reported for LgtC[17]and underscores the evolutionary optimization of nucleotide-sugar donors for catalytic engagement. The high occupancy of these polar contacts throughout the trajectory confirms that the donor site remains structurally rigid under physiological conditions, serving as a benchmark for evaluating analogues. In contrast, thioglycoside analogues such as FucSBn and BacSBn preserved donor-side hydrogen bonds but shifted their stabilization strategy toward hydrophobic and π-driven interactions. Both compounds exhibited persistent π–alkyl and π–π contacts involving their benzyl aglycones, as well as sulfur-assisted dispersion interactions that compensate for the absence of phosphate groups. This behavior aligns with prior reports on non-substrate LgtC inhibitors, where aglycone anchoring and induced fit contribute to competitive inhibition without nucleotide tails.[30] The persistence of these contacts during MD suggests that thioglycosides exploit microcavities adjacent to the donor cleft, a phenomenon previously documented for GT-B enzymes.[20]

Among the screened analogues, C-5, C-14, and C-18 emerged as the most dynamically stable candidates. These ligands

combined a donor-like hydrogen-bond spine with extensive π-stacking and π–alkyl interactions, reinforced by sulfur-centered contacts that remained cooperative throughout the simulation. Notably, C-18 demonstrated deep hydrophobic seating and multipoint aromatic engagement; while maintaining at least one high-occupancy H-bond to catalytic residues, an interaction pattern that has been associated in previous GT-B studies with stable binding.[20,30] The redistribution of interaction energy from purely electrostatic to mixed polar–dispersion contributions reflect an induced-fit mechanism, consistent with structural plasticity observed in glycosyltransferases during ligand binding[17]. Collectively, these findings validate the design logic of thioglycoside analogues and highlight the role of aglycone-driven stabilization in achieving competitive inhibition of LgtC.

To complement the qualitative analysis of equilibrium interactions, Table 4 summarizes the key interaction types, hydrogen bonds, π-contacts, and sulfur-mediated interactions, observed for each ligand in both the docking snapshot and MD equilibrium state. This comparative view highlights how initial docking predictions translate into persistent contacts under dynamic conditions.

The table 4 summarizes three key interaction classes, hydrogen bonds, π-contacts (π–π and π–alkyl), and sulfur-mediated interactions, for the natural donor (UDP-Gal), reference thioglycosides (FucSBn, BacSBn), and selected analogues (C-series). Interaction counts are expressed qualitatively as High (≥4), Medium (2–3), or Low (0–1), based on docking predictions and MD persistence (≥30% occupancy). Sulfur interactions include S···π and S···O contacts, which are absent in the natural ligand but consistently present in thioglycosides.

Table 4. Comparative interaction profiles for ligands bound to LgtC under docking and MD equilibrium conditions.

Ligand	Docking H-bonds	Docking π-contacts	Docking S-interactions	MD H-bonds	MD π-contacts	MD S-interactions
Natural ligand	High (4–6)	Low–Med (1–2)	-	High (3–5)	Low–Med (1–2)	-
FucSBn	Med (2–3)	Med–High (2–4)	Present	Med (2–3)	Med–High (2–4)	Present
BacSBn	Med (2–3)	High (3–4)	Present	Med (2–3)	High (3–4)	Present
C-1	Med (2–3)	Low–Med (1–2)	Present	Med (2–3)	Low–Med (1–2)	Present
C-4	Med (2–3)	High (3–4)	Present	Low–Med (1–2)	High (3–4)	Present
C-5	Med (2–3)	High (3–5)	Present	Low–Med (1–2)	High (4–5)	Present
C-6	Med (2–3)	Low–Med (1–2)	Present	Med (2–3)	Low–Med (1–2)	Present
C-7	Med (2–3)	Low–Med (1–2)	Present	Med (2–3)	Low–Med (1–2)	Present
C-12	Med (2–3)	Low–Med (1–2)	Present	Med (2–3)	Low–Med (1–2)	Present
C-13	Med (2–3)	Med–High (3–4)	Present	Med (2–3)	Med–High (3–4)	Present
C-14	Med (2–3)	Med–High (3–4)	Present	Med (2–3)	Med–High (3–4)	Present
C-18	Low–Med (1–2)	High (4–6)	Present	Low–Med (1–2)	High (4–6)	Present

The comparative analysis between docking and MD equilibrium highlights how initial predictions translate into dynamic stability. Docking provided a static estimate of interaction potential, identifying key hydrogen bonds and hydrophobic contacts

expected to anchor ligands within the LgtC catalytic pocket. However, MD simulations reveal which of these interactions persist under physiological conditions, offering a more realistic view of binding behavior.

For the natural ligand, the persistence of a phosphate-centered hydrogen-bond network and minimal pose drift confirms that the docking pose closely approximates the crystallographic orientation. This agreement validates the docking protocol and establishes a benchmark for donor-like positioning. Thioglycoside analogues such as FucSBn and BacSBn also retained their predicted donor-side hydrogen bonds while reinforcing stability through π-stacking and sulfur-mediated contacts. In contrast, for compounds C-1, C-6, C-7, C-12) they preserve 2–3 H-bonds and add modest π-support, yielding conservative, donor-like stabilization consistent with GT-B recognition principles.[1738] On the other hand, C-4, C-5, C-18), They relinquish some polar contacts yet develop dense π networks and S-mediated interactions that persist through MD, a hallmark of induced-fit seating in GT-B donor clefts.[2030] Finally, C-13 and C-14 retain the donor-side H-bond spine while reinforcing the aglycone π-stack, a profile frequently associated with favorable MM/GBSA trends in LgtC campaigns[30.2030] This adaptive behavior indicates that the docking poses were not only plausible but also positioned for the ligands to exploit induced-fit mechanisms during equilibration.

Docking and molecular dynamics (MD) simulations jointly indicate that thioglycoside analogs, including FucSBn, BacSBn, and selected C-series compounds, can occupy the donor (UDP-sugar) pocket of LgtC in poses that overlap with the crystallographic binding mode of UDP-α-D-galactose (PDB ID: 1GA8[17]). This spatial overlap strongly suggests an active-site engagement rather than allosteric binding. The analogues reproduce key donor-recognition features through 2–3 persistent hydrogen bonds involving the sugar and amide moieties, while achieving additional stabilization via π–π and π–alkyl interactions and sulfur-mediated contacts (S···π, S···O) between their aromatic aglycones and hydrophobic subpockets. These interaction patterns align with established GT-B glycosyltransferase recognition principles, where donor binding relies on a phosphate/ribose hydrogen-bond spine and nucleobase stacking, complemented by induced-fit adjustments during catalysis[20].

Mechanistically, the binding process can be rationalized in four steps. First, the sugar moiety of each analogue engages the donor cleft in a donor-like configuration, mimicking the hydrogen-bond network typically formed by the phosphate and ribose groups of UDP-Gal[17]. Second, the benzyl or aryl aglycone occupies a π-rich subpocket, forming π–π and π–alkyl contacts, while the thio-linkage introduces S···π and S···O interactions, leveraging sulfur's polarizability to reinforce binding[20]. Third, unlike UDP, these analogues lack the uridine–pyrophosphate moiety and cannot undergo glycosyl transfer. Their occupation of the donor site sterically and electronically prevents productive binding of the natural substrate, resulting in competitive inhibition.[30] Finally, MD trajectories confirm that these interaction networks remain stable over time, with minimal pose drift and sustained contact frequencies, criteria that distinguish genuine stabilizing interactions from docking artifacts.[38]

From a functional perspective, these compounds seem acting as antagonists rather than agonists. LgtC is an enzyme, not a receptor; ligands cannot "activate" it unless they serve as chemically competent donors. Thioglycoside analogues lack catalytic functionality and therefore behave as competitive inhibitors, attenuating LOS biosynthesis by blocking donor-site access.[2030] The persistence of donor-like hydrogen bonds combined with π and sulfur contacts supports an active-site binding mode, reinforcing the hypothesis that these molecules interfere directly with the catalytic itinerary rather than exerting allosteric modulation.

Although these findings are derived from in *silico* analyses, the consistency between docking and MD observations supports the plausibility of the predicted binding modes. The observed stability patterns, i.e., low RMSD, high hydrogen-bond occupancy, and cooperative π/S interactions, suggest that these scaffolds represent credible starting points for lead optimization. By exploiting donor mimicry and aglycone-driven stabilization, thioglycoside analogues offer a promising framework for the design of next-generation glycosyltransferase inhibitors, addressing an urgent need for novel strategies against multidrug-resistant Gram-negative pathogens.

3. Materials and methods.

3.1 Data collection.

The main objective of this study was to identify novel metabolic decoys with high selectivity and strong binding affinity toward bacterial glycosyltransferases. Such compounds were expected to act as competitive inhibitors, enabling sustained and cumulative suppression of enzymatic activity. For this goal, the data collection starts searching similarity compounds to FucSBn (CID: 171378782) and BacSBn (CID: 171378781). To identify structural analogs of the reference, we employed the PubChem Similarity Search tool (https://pubchem.ncbi.nlm.nih.gov accesed on september 2025), which provides two complementary approaches: 2D similarity based on molecular fingerprints and 3D similarity based on shape and feature overlays. The 2D method relies on binary molecular fingerprints, which encode the presence or absence of predefined substructures as a string of bits (0 or 1). Each bit represents a specific chemical feature, such as a functional group or ring system, allowing rapid comparison of molecular topologies.[55] Similarity between the query compound and database entries is quantified using the Tanimoto coefficient, calculated as (1):

$$T = \frac{c}{a+b-c} - T = \frac{c}{a+b-c}$$ Equation 1.

Where a and b are the number of bits set in each fingerprint, and c is the number of bits common to both. This metric is widely accepted in cheminformatics for fingerprint-based similarity due to its robustness and discriminatory power.[55,56] For this study, we applied a similarity threshold of ≥ 0.85, ensuring high structural resemblance while permitting minor variations that could enhance binding affinity. On the other hand, the 3D similarity approach evaluates molecular shape and pharmacophoric features using conformer ensembles generated for each compound. PubChem implements an algorithm based on ROCS (Rapid Overlay of Chemical Structures), which overlays molecular shapes and compares feature distributions to compute a similarity score.[57] This method captures steric and electrostatic complementarity, which is critical for predicting binding interactions in enzyme active sites.

Both similarity modes were used to retrieve candidate molecules from PubChem. The resulting analogs, with threshold of ≥ 0.85 were ranked by descending similarity score, and those meeting the predefined threshold were exported in SDF format for subsequent minimum energy calculation (optimization), docking and molecular dynamics simulations respectively. Additional filtering was applied based on drug-likeness criteria and removal of PAINS (Pan-Assay Interference Compounds) alerts.

3.2 Minimum energies structures.

After retrieving both the reference compound and its structural analogs from the PubChem database, their lowest-energy conformations were determined through a two-step protocol. First, the downloaded SDF files were imported into Avogadro 2.0, where conformational sampling was performed using a genetic algorithm to explore the torsional space and identify the most probable conformers. The conformer with the lowest estimated energy was then selected for further refinement. Next, these preliminary structures were converted to PDB format and optimized using Gaussian 09 for linux. Geometry optimization was carried out at the PM6 semi-empirical level of theory, ensuring proper consideration of stereochemistry and minimizing intramolecular strain. This step provided a more accurate representation of the electronic structure while maintaining computational efficiency. The optimized conformers were saved again in PDB format for subsequent ADme-Tox filters, molecular docking, and molecular dynamics simulations.

3.3 ADME-Tox properties calculations.

ADME-Tox properties, Absorption, Distribution, Metabolism, Excretion, and Toxicity, are fundamental parameters in the evaluation of bioactive compounds, as they determine pharmacokinetic behavior and safety profiles within the organism. Their early assessment is particularly relevant for molecules with complex structural features, such as glycosides or peptide-like analogs, which often exhibit variability in bioavailability, metabolic stability, and toxicity.[58] Evaluating these properties at the initial stages of drug discovery significantly reduces the risk of failure in later clinical phases, optimizing resource allocation and improving overall success rates.[59] Therefore, this approach enables the early exclusion of compounds with poor therapeutic viability due to unfavorable pharmacokinetics or toxicity concerns, thereby minimizing experimental costs and accelerating the identification of safer candidates.[60]

In this study, toxicity profiling of thioglycoside analogs was performed using ProTox-II[34], a machine-learning-based platform that predicts multiple safety endpoints, including acute oral toxicity (LD50), hepatotoxicity, mutagenicity, carcinogenicity, and immunotoxicity. Each compound was submitted in SMILES format, and results were exported in CSV for comparative analysis. Classification thresholds were established according to the Globally Harmonized System (GHS) and validated against preclinical reference values: compounds with LD50 > 5000 mg/kg were considered non-toxic, while those between 2000–5000

mg/kg were classified as moderately toxic.[60] By integrating these predictive models into the screening workflow, we enhance the reliability of in silico toxicity profiling and reduce the likelihood of advancing unsafe compounds to experimental or clinical stages, ultimately improving the efficiency of the drug discovery pipeline.[59]

3.4 Target Selection.

The rapid rise of multidrug-resistant bacteria has created an urgent need for new therapeutic strategies that move beyond traditional antibiotic targets. Among the promising alternatives are bacterial glycosyltransferases, enzymes essential for cell envelope biosynthesis. LgtC, an α-1,4-galactosyltransferase, plays a critical role in the assembly of lipooligosaccharides (LOS), which are key structural components of the outer membrane in several Gram-negative pathogens. Disruption of this pathway compromises membrane integrity and impairs immune evasion, ultimately reducing bacterial viability and virulence[17,61] What makes LgtC particularly attractive is that it remains largely underexploited as an antibacterial target. Unlike many conventional targets, LgtC has no close human homologs, minimizing the risk of off-target effects.[62] Furthermore, because inhibitors of LgtC would primarily attenuate virulence rather than exert strong bactericidal pressure, they could reduce the selective forces that drive resistance development.[63,64] Recent structural studies and early inhibitor designs have demonstrated the tractability of this enzyme for drug discovery.[30,65] Taken together, these features position LgtC as a biologically essential, structurally characterized, and underutilized target with significant potential to contribute to the next generation of antibacterial agents.

3.5 Molecular docking.

Molecular docking has become a cornerstone of structure-based drug design (SBDD), enabling researchers to predict how small molecules (ligands) interact with biological macromolecules such as proteins or nucleic acids. By simulating the binding process at the atomic level, docking provides insights into the orientation, conformation, and binding affinity of candidate compounds within the active site of a target. This predictive capability is essential for rational drug design, as it allows the identification of promising leads before costly experimental validation.[66]

The primary advantage of molecular docking lies in its ability to accelerate drug discovery by reducing time and cost compared to traditional high-throughput screening. Docking algorithms explore multiple ligand conformations and orientations, ranking them based on scoring functions that estimate binding free energy. These computational predictions guide medicinal chemists in optimizing molecular structures for improved potency, selectivity, and pharmacokinetic properties.[67] Beyond lead identification, docking plays a critical role in virtual screening of large compound libraries, drug repurposing, and understanding molecular recognition processes. It is widely applied in therapeutic areas such as oncology, neurodegenerative diseases, infectious diseases, and metabolic disorders. The integration of docking with other computational techniques, such as molecular dynamics and free energy calculations, further enhances its predictive accuracy, making it a vital component of modern drug development pipelines.[68]

In this work, molecular docking was performed to evaluate the interactions between the selected thioglycoside analogs and the bacterial glycosyltransferase LgtC. Docking simulations were carried out using AutoDock Vina 2.0 and AutoDock-GPU 2.0 under a Linux operating system. Although AutoDock Vina has demonstrated its reliability in studying diverse ligand classes, including small molecules, nucleic acids, and peptides, with protein targets[69], the combination of AutoDock-GPU with the adaptive ADADELTA algorithm offers superior performance for highly flexible systems, such as those investigated in this study.[70] Besides, AutoDock-GPU significantly accelerates docking calculations by leveraging GPU parallelization, achieving speed-ups of up to 170-fold compared to traditional CPU-based approaches. This computational advantage is critical when screening large sets of analogs retrieved from PubChem similarity searches, where exhaustive sampling of ligand conformations is required. Furthermore, the ADADELTA-based local search improves convergence efficiency, particularly for ligands with multiple rotatable bonds, ensuring accurate pose prediction and robust binding energy estimation.[71] Therefore, all results reported in this study were generated using AutoDock-GPU as the primary docking engine, enabling efficient and reliable virtual screening of structurally diverse thioglycoside analogs. The binding affinity was evaluated by means of the score value, where a more negative value represents better docking.

3.6 Ligand and protein preparation.

The selected ligands were subjected to a structural preprocessing protocol to ensure compatibility and accuracy in molecular docking simulations. Initially, each ligand structure was curated by removing unwanted molecules, residual ions, and solvent fragments that could interfere with binding predictions. Kollman partial charges were then calculated and assigned, as these charges provide a computationally efficient approximation of electrostatic interactions for small molecules.[72] After completing

these steps, the ligands were converted to PDBQT format, the standard required by docking engines such as AutoDock Vina and AutoDock-GPU. On the other hand, the target protein, glycosyltransferase LgtC, was retrieved from the RCSB Protein Data Bank under accession code 1GA8[17]. Protein preparation involves removing non-essential components, such as crystallographic water molecules and ligands that are not involved in catalysis. Gasteiger charges[73] were assigned to the protein to accurately represent its electrostatic environment, as these charges are widely used in AutoDock protocols for macromolecules. Finally, the prepared protein was converted and stored in PDBQT format, maintaining consistency and compatibility throughout the computational workflow.

3.7 Docking protocol.

Docking simulations were performed to predict the binding interactions between the selected thioglycoside analogs and the bacterial glycosyltransferase LgtC. The protein structure was obtained from the RCSB Protein Data Bank (PDB ID: 1GA8).[74] The docking grid was centered on the active site previously reported for LgtC, ensuring accurate sampling of the catalytic pocket. The coordinates and box dimensions used for the docking procedure are shown in table 5.

Table 5. Docking parameter employed in this work

Structure	X Center	X Size	Y Center	Y Size	Z Center	Z Size
LgtC	27	50	51	50	61	50

These parameters were selected to encompass all residues involved in glycosyl transfer, providing sufficient space for ligand flexibility during docking. Then, docking procedure was executed using a customized script based on AutoDock-GPU Vina 2.0, under a Linux environment. The ADADELTA local search algorithm, a first-order gradient-based optimization method, was employed due to its proven efficiency in exploring complex conformational spaces.[70] For each ligand, 100 distinct conformations were generated per run, with a maximum of 42,000 generations and 2,500,000 evaluations per execution of the Lamarckian Genetic Algorithm (LGA). These parameters ensured robust sampling of the conformational search space and reliable estimation of binding affinities.

The resulting docking poses were ranked according to predicted binding free energy (scoring values, in kcal/mol), and the top-scoring conformations were analyzed for key interactions, including hydrogen bonding, hydrophobic contacts, and π-stacking, using PyMOL (3.1.6.1) and Discovery studio Visualizer (v25.1.0.24284).

3.8 Molecular Dynamics.

Molecular Dynamics (MD) simulations have become an indispensable tool in modern drug discovery, offering insights that go beyond static docking predictions. While docking provides an initial estimate of ligand binding affinity and orientation, MD simulations allow researchers to explore the dynamic behavior of protein-ligand complexes over time, under conditions that mimic physiological environments. This approach captures conformational flexibility, solvent effects, and entropic contributions, which are critical for understanding binding stability and mechanism of action.[75] The ability of MD to model atomic-level interactions in real time makes it particularly valuable for refining docking results, validating binding poses, and predicting kinetic properties such as residence time. These simulations also help identify induced-fit effects and allosteric changes that cannot be captured by rigid docking protocols. Consequently, MD has been widely applied in lead optimization, structure-based drug design, and fragment-based screening.[76–78] Successful drug discovery projects have leveraged MD simulations to advance candidate molecules. For example: HIV protease inhibitors were optimized using MD to understand flap dynamics and improve binding stability.[79] In other work, MD studies contributed to the design of kinase inhibitors by revealing transient binding pockets and water-mediated interactions.[80] In the development of COVID-19 antivirals, MD simulations were used to validate docking predictions and assess the stability of inhibitors targeting SARS-CoV-2 main protease.[81] By integrating MD into the computational pipeline, researchers can reduce false positives from docking, prioritize compounds with robust dynamic stability, and gain mechanistic insights that guide rational drug design. This synergy between docking and MD enhances predictive accuracy and accelerates the discovery of clinically relevant molecules.[82]

After applying ADME-Tox filters and selecting ligands with the most favorable docking scores, the top-ranked protein–ligand complexes were subjected to Molecular Dynamics (MD) simulations to evaluate their stability under near-physiological conditions. Simulations were performed using YASARA Dynamics v32.12.24 with the AMBER14 force field, which has been extensively validated for protein–ligand interaction studies.[38] Each complex was placed in a cubic simulation box with a 5 Å

margin around the solute and periodic boundary conditions (PBC) applied to mimic an infinite system. The environment was parameterized to reflect physiological conditions: pH: 7.4, Temperature: 298 K, NaCl concentration: 0.9% for system neutralization, Water density: 0.997 g/mL. Pressure was dynamically regulated by adjusting the box volume according to solvent density, simulating intracellular pressure conditions relevant to bacterial environments. Each MD run was executed for 100 nanoseconds (ns), ensuring sufficient sampling of conformational dynamics. The integration time step was set to 2 fs, and long-range electrostatics were treated using the Particle Mesh Ewald (PME) method.

Upon completion, structural stability was assessed using the md_analyze_dynamics.mcr macro in YASARA, extracting metrics such as Root Mean Square Deviation (RMSD) and Root Mean Square Fluctuation (RMSF) to monitor conformational changes over time. Binding free energies were calculated using the md_analyzebindenergy.mcr macro, which employs a modified MM/PBSA methodology. In YASARA, the polar solvation energy is estimated through the Adaptive Poisson–Boltzmann Solvation (APBS) approach. This method does not explicitly include entropic contributions; however, an approximate correction is applied by accounting for the surface entropy cost, based on a predefined parameter of 0.65 kJ·mol·Å. This parameter also incorporates the van der Waals interaction energies between the solvent and the solute. Together, these adjustments provide a nearly complete MM/PBSA-based estimation of binding free energy. The resulting values were interpreted according to the thermodynamic definition of binding energy.[83–86]

$$\Delta G_{Bind} = G_{Complex} - (G_{Protein} + G_{Ligand})$$ Equation 2.

The MM/PBSA-based ΔG_{bind} values follow the standard thermodynamic convention in which more negative energies correspond to stronger binding, correlating with greater stabilization of the complex and, in principle, with higher therapeutic potential. This analysis allowed comparison of candidate ligands against natural substrates of glycosyltransferases.

Conclusions.

This *in silico* study identifies thioglycoside analogues as credible donor-site binders of LgtC, a key glycosyltransferase involved in lipooligosaccharide biosynthesis in Gram-negative bacteria. Using a workflow that integrates similarity-based ligand selection, ADME–Tox filtering, molecular docking, and long-timescale molecular dynamics simulations, we uncovered compounds that stably engage the UDP-galactose donor pocket. These analogues mimic critical donor interactions such as hydrogen bonding with catalytic residues, and introduce additional stabilizing features, including π-stacking and sulfur-mediated contacts, which persist throughout the simulations. This binding profile supports a putative competitive inhibition mechanism, in which thioglycosides occlude the donor site and prevent substrate access. While these findings are derived from computational models, the convergence of docking and MD results lends confidence to the biological plausibility of the predicted binding modes. These data provide a rational basis for experimental validation. Future work should prioritize enzymatic assays to confirm inhibitory activity, SAR studies to optimize aglycone–protein contacts, and permeability testing in Gram-negative models to assess compound uptake. Overall, thioglycoside analogs represent a computationally supported framework that could guide the future development of donor-site–targeted glycosyltransferase inhibitors against multidrug-resistant Gram-negative pathogens.

Data availability: All data generated or analysed during this study are included in this published article, and its supplementary information files

References

1. Gilham, E. L., Pearce-Smith, N., Carter, V. & Ashiru-Oredope, D. Assessment of global antimicrobial resistance campaigns conducted to improve public awareness and antimicrobial use behaviours: a rapid systematic review. *BMC Public Health* **24**, 396 (2024).
2. Sijbom, M., Büchner, F. L., Saadah, N. H., Numans, M. E. & De Boer, M. G. J. Trends in antibiotic selection pressure generated in primary care and their association with sentinel antimicrobial resistance patterns in Europe. *Journal of Antimicrobial Chemotherapy* **78**, 1245–1252 (2023).
3. Salam, Md. A. *et al.* Antimicrobial Resistance: A Growing Serious Threat for Global Public Health. *Healthcare* **11**, 1946 (2023).
4. Hughes, D. Selection and evolution of resistance to antimicrobial drugs. *IUBMB Life* **66**, 521–529 (2014).
5. Albrich, W. C., Monnet, D. L. & Harbarth, S. Antibiotic Selection Pressure and Resistance in *Streptococcus pneumoniae* and *Streptococcus pyogenes*. *Emerg Infect Dis* **10**, 514–517 (2004).

6. Kealey, C., Creaven, C. A., Murphy, C. D. & Brady, C. B. New approaches to antibiotic discovery. *Biotechnol Lett* **39**, 805–817 (2017).
7. Jackson, N., Czaplewski, L. & Piddock, L. J. V. Discovery and development of new antibacterial drugs: learning from experience? *Journal of Antimicrobial Chemotherapy* **73**, 1452–1459 (2018).
8. Liu, F. *et al.* Antibacterial activity of recently approved antibiotics against methicillin-resistant Staphylococcus aureus (MRSA) strains: A systematic review and meta-analysis. *Ann Clin Microbiol Antimicrob* **21**, 37 (2022).
9. Terreni, M., Taccani, M. & Pregnolato, M. New Antibiotics for Multidrug-Resistant Bacterial Strains: Latest Research Developments and Future Perspectives. *Molecules* **26**, 2671 (2021).
10. Dalbanjan, N. P. & Praveen Kumar, S. K. A Chronicle Review of In-Silico Approaches for Discovering Novel Antimicrobial Agents to Combat Antimicrobial Resistance. *Indian J Microbiol* **64**, 879–893 (2024).
11. Atasever, S. In silico drug discovery: a machine learning-driven systematic review. *Medicinal Chemistry Research* **33**, 1465–1490 (2024).
12. Preston, A., Mandrell, R. E., Gibson, B. W. & Apicella, M. A. The Lipooligosaccharides of Pathogenic Gram-Negative Bacteria. *Crit Rev Microbiol* **22**, 139–180 (1996).
13. Bertani, B. & Ruiz, N. Function and Biogenesis of Lipopolysaccharides. *EcoSal Plus* **8**, (2018).
14. Gronow, S. & Brade, H. Lipopolysaccharide biosynthesis: which steps do bacteria need to survive? *J Endotoxin Res* **7**, 3–23 (2001).
15. Chen, Y. *et al.* Crystal structure of the lipopolysaccharide outer core galactosyltransferase WaaB involved in pathogenic bacterial invasion of host cells. *Front Microbiol* **14**, (2023).
16. Danaher, R. J. *et al.* Genetic basis of Neisseria gonorrhoeae lipooligosaccharide antigenic variation. *J Bacteriol* **177**, 7275–7279 (1995).
17. Persson, K. *et al.* Crystal structure of the retaining galactosyltransferase LgtC from Neisseria meningitidis in complex with donor and acceptor sugar analogs. *Nat Struct Biol* **8**, 166–175 (2001).
18. Šnajdrová, L., Kulhánek, P., Imberty, A. & Koča, J. Molecular dynamics simulations of glycosyltransferase LgtC. *Carbohydr Res* **339**, 995–1006 (2004).
19. Quintana, I. de la L. *et al.* Thioglycosides Act as Metabolic Inhibitors of Bacterial Glycan Biosynthesis. *ACS Infect Dis* **9**, 2025–2035 (2023).
20. Kim, Y. *et al.* Thioglycoligase-Based Assembly of Thiodisaccharides: Screening as β-Galactosidase Inhibitors. *ChemBioChem* **8**, 1495–1499 (2007).
21. Kim, S., Bolton, E. E. & Bryant, S. H. Similar compounds versus similar conformers: complementarity between PubChem 2-D and 3-D neighboring sets. *J Cheminform* **8**, 62 (2016).
22. Crunkhorn, S. Designing new antibiotics. *Nat Rev Drug Discov* **24**, 827–827 (2025).
23. Krishnan, A. *et al.* A generative deep learning approach to de novo antibiotic design. *Cell* **188**, 5962-5979.e22 (2025).
24. Dehbanipour, R. & Ghalavand, Z. Anti-virulence therapeutic strategies against bacterial infections: recent advances. *Germs* **12**, 262–275 (2022).
25. Fleitas Martínez, O., Cardoso, M. H., Ribeiro, S. M. & Franco, O. L. Recent Advances in Anti-virulence Therapeutic Strategies With a Focus on Dismantling Bacterial Membrane Microdomains, Toxin Neutralization, Quorum-Sensing Interference and Biofilm Inhibition. *Front Cell Infect Microbiol* **9**, (2019).
26. Tay, S. & Yew, W. Development of Quorum-Based Anti-Virulence Therapeutics Targeting Gram-Negative Bacterial Pathogens. *Int J Mol Sci* **14**, 16570–16599 (2013).
27. Dickey, S. W., Cheung, G. Y. C. & Otto, M. Different drugs for bad bugs: antivirulence strategies in the age of antibiotic resistance. *Nat Rev Drug Discov* **16**, 457–471 (2017).
28. Rasko, D. A. & Sperandio, V. Anti-virulence strategies to combat bacteria-mediated disease. *Nat Rev Drug Discov* **9**, 117–128 (2010).
29. Bertani, B. & Ruiz, N. Function and Biogenesis of Lipopolysaccharides. *EcoSal Plus* **8**, (2018).
30. Ema, M., Xu, Y., Gehrke, S. & Wagner, G. K. Identification of non-substrate-like glycosyltransferase inhibitors from library screening: pitfalls & hits. *Medchemcomm* **9**, 131–137 (2018).
31. Acosta Gutiérrez, S., Bodrenko, I. & Ceccarelli, M. Permeability Through Bacterial Porins Dictates Whole Cell Compound Accumulation. Preprint at https://doi.org/10.26434/chemrxiv.11877834.v1 (2020).
32. Krishnamoorthy, G. *et al.* Synergy between Active Efflux and Outer Membrane Diffusion Defines Rules of

Antibiotic Permeation into Gram-Negative Bacteria. *mBio* **8**, (2017).
33. Acosta-Gutiérrez, S., Bodrenko, I. & Ceccarelli, M. The Influence of Permeability through Bacterial Porins in Whole-Cell Compound Accumulation. *Antibiotics* **10**, 635 (2021).
34. Banerjee, P., Kemmler, E., Dunkel, M. & Preissner, R. ProTox 3.0: a webserver for the prediction of toxicity of chemicals. *Nucleic Acids Res* **52**, W513–W520 (2024).
35. Hodgson, J. ADMET—turning chemicals into drugs. *Nat Biotechnol* **19**, 722–726 (2001).
36. Persson, K. *et al.* Crystal structure of the retaining galactosyltransferase LgtC from Neisseria meningitidis in complex with donor and acceptor sugar analogs. *Nat Struct Biol* **8**, 166–175 (2001).
37. Chowdhary, R. *et al.* Synthesis, Characterization, and Antimicrobial Activity of Ultra-Short Cationic β-Peptides. *ACS Infect Dis* **9**, 1437–1448 (2023).
38. Forli, S. *et al.* Computational protein–ligand docking and virtual drug screening with the AutoDock suite. *Nat Protoc* **11**, 905–919 (2016).
39. Bell, E. W. & Zhang, Y. DockRMSD: an open-source tool for atom mapping and RMSD calculation of symmetric molecules through graph isomorphism. *J Cheminform* **11**, 40 (2019).
40. Zhou, C. *et al.* GTDB: an integrated resource for glycosyltransferase sequences and annotations. *Database* **2020**, (2020).
41. Lobanov, M. Yu., Bogatyreva, N. S. & Galzitskaya, O. V. Radius of gyration as an indicator of protein structure compactness. *Mol Biol* **42**, 623–628 (2008).
42. Elebiju, O. F., Oduselu, G. O., Ogunnupebi, T. A., Ajani, O. O. & Adebiyi, E. In Silico Design of Potential Small-Molecule Antibiotic Adjuvants against Salmonella typhimurium Ortho Acetyl Sulphydrylase Synthase to Address Antimicrobial Resistance. *Pharmaceuticals* **17**, 543 (2024).
43. Hassan, A. M. *et al.* Evaluating the Binding Potential and Stability of Drug-like Compounds with the Monkeypox Virus VP39 Protein Using Molecular Dynamics Simulations and Free Energy Analysis. *Pharmaceuticals* **17**, 1617 (2024).
44. Lobanov, M. Yu., Bogatyreva, N. S. & Galzitskaya, O. V. Radius of gyration as an indicator of protein structure compactness. *Mol Biol* **42**, 623–628 (2008).
45. Adelusi, T. I. *et al.* Molecular modeling in drug discovery. *Inform Med Unlocked* **29**, 100880 (2022).
46. Chowdhury, R. *et al.* In-Silico discovery of novel cephalosporin antibiotic conformers via ligand-based pharmacophore modelling and de novo molecular design. *Journal of Genetic Engineering and Biotechnology* **23**, 100514 (2025).
47. Shukla, R. & Tripathi, T. Molecular Dynamics Simulation of Protein and Protein–Ligand Complexes. in *Computer-Aided Drug Design* 133–161 (Springer Singapore, Singapore, 2020). doi:10.1007/978-981-15-6815-2_7.
48. Brueckner, A. C. *et al.* MDFit: automated molecular simulations workflow enables high throughput assessment of ligands-protein dynamics. *J Comput Aided Mol Des* **38**, 24 (2024).
49. Genheden, S. & Ryde, U. The MM/PBSA and MM/GBSA methods to estimate ligand-binding affinities. *Expert Opin Drug Discov* **10**, 449–461 (2015).
50. Wang, Y. *et al.* Retro Drug Design: From Target Properties to Molecular Structures. *J Chem Inf Model* **62**, 2659–2669 (2022).
51. Shukla, R. & Tripathi, T. Molecular Dynamics Simulation in Drug Discovery: Opportunities and Challenges. in *Innovations and Implementations of Computer Aided Drug Discovery Strategies in Rational Drug Design* 295–316 (Springer Singapore, Singapore, 2021). doi:10.1007/978-981-15-8936-2_12.
52. Smirnovienė, J., Baranauskienė, L., Zubrienė, A. & Matulis, D. A standard operating procedure for an enzymatic activity inhibition assay. *European Biophysics Journal* **50**, 345–352 (2021).
53. Schutzbach, J. & Brockhausen, I. Inhibition of Glycosyltransferase Activities as the Basis for Drug Development. in *Glycomics* 359–373 (Humana Press, Totowa, NJ, 2009). doi:10.1007/978-1-59745-022-5_25.
54. Tvaroška, I. Glycosyltransferases as targets for therapeutic intervention in cancer and inflammation: molecular modeling insights. *Chemical Papers* **76**, 1953–1988 (2022).
55. Bajusz, D., Rácz, A. & Héberger, K. Why is Tanimoto index an appropriate choice for fingerprint-based similarity calculations? *J Cheminform* **7**, 20 (2015).
56. Alcázar, J. J. *et al.* A Simple Machine Learning-Based Quantitative Structure–Activity Relationship Model

for Predicting pIC50 Inhibition Values of FLT3 Tyrosine Kinase. *Pharmaceuticals* **18**, 96 (2025).
57. Sauer, W. H. B. & Schwarz, M. K. Molecular Shape Diversity of Combinatorial Libraries: A Prerequisite for Broad Bioactivity. *J Chem Inf Comput Sci* **43**, 987–1003 (2003).
58. Boström, J. & Brown, D. G. Stuck in a rut with old chemistry. *Drug Discov Today* **21**, 701–703 (2016).
59. Theuretzbacher, U. Antibacterial innovation in European SMEs. *Nat Rev Drug Discov* **15**, 812–813 (2016).
60. Nightingale, A. *et al.* The Proteins API: accessing key integrated protein and genome information. *Nucleic Acids Res* **45**, W539–W544 (2017).
61. Banerjee, A. *et al.* Identification of the gene (*lgtG*) encoding the lipooligosaccharide β chain synthesizing glucosyl transferase from *Neisseria gonorrhoeae*. *Proceedings of the National Academy of Sciences* **95**, 10872–10877 (1998).
62. Jackson, M. D., Wong, S. M. & Akerley, B. J. Underlying Glycans Determine the Ability of Sialylated Lipooligosaccharide To Protect Nontypeable Haemophilus influenzae from Serum IgM and Complement. *Infect Immun* **87**, (2019).
63. Yakovlieva, L., Fülleborn, J. A. & Walvoort, M. T. C. Opportunities and Challenges of Bacterial Glycosylation for the Development of Novel Antibacterial Strategies. *Front Microbiol* **12**, (2021).
64. Theuretzbacher, U., Blasco, B., Duffey, M. & Piddock, L. J. V. Unrealized targets in the discovery of antibiotics for Gram-negative bacterial infections. *Nat Rev Drug Discov* **22**, 957–975 (2023).
65. Xu, Y. & Wagner, G. K. A cell-permeable probe for the labelling of a bacterial glycosyltransferase and virulence factor. *RSC Chem Biol* **5**, 55–62 (2024).
66. Ferreira, L., Dos Santos, R., Oliva, G. & Andricopulo, A. Molecular Docking and Structure-Based Drug Design Strategies. *Molecules* **20**, 13384–13421 (2015).
67. Nivatya, H. K. *et al.* Assessing molecular docking tools: understanding drug discovery and design. *Futur J Pharm Sci* **11**, 111 (2025).
68. Author, C. & Bhowate, S. H. | Review. *Int. J. in Pharm. Sci* **1**, 170–181 (2023).
69. Trott, O. & Olson, A. J. AutoDock Vina: Improving the speed and accuracy of docking with a new scoring function, efficient optimization, and multithreading. *J Comput Chem* **31**, 455–461 (2010).
70. Santos-Martins, D., Solis-Vasquez, L., Koch, A. & Forli, S. Accelerating AutoDock4 with GPUs and Gradient-Based Local Search. Preprint at https://doi.org/10.26434/chemrxiv.9702389.v1 (2019).
71. Tang, S. *et al.* Accelerating AutoDock Vina with GPUs. *Molecules* **27**, 3041 (2022).
72. Singh, U. C. & Kollman, P. A. An approach to computing electrostatic charges for molecules. *J Comput Chem* **5**, 129–145 (1984).
73. Gasteiger, J. & Marsili, M. A new model for calculating atomic charges in molecules. *Tetrahedron Lett* **19**, 3181–3184 (1978).
74. CRYSTAL STRUCTURE OF GALACOSYLTRANSFERASE LGTC IN COMPLEX WITH DONOR AND ACCEPTOR SUGAR ANALOGS. Preprint at https://doi.org/10.2210/pdb1ga8/pdb (2001).
75. Salo-Ahen, O. M. H. *et al.* Molecular Dynamics Simulations in Drug Discovery and Pharmaceutical Development. *Processes* **9**, 71 (2020).
76. Gu, S. *et al.* Can molecular dynamics simulations improve predictions of protein-ligand binding affinity with machine learning? *Brief Bioinform* **24**, (2023).
77. Lukauskis, D. *et al.* Open Binding Pose Metadynamics: An Effective Approach for the Ranking of Protein–Ligand Binding Poses. *J Chem Inf Model* **62**, 6209–6216 (2022).
78. Defelipe, L. A. *et al.* Solvents to Fragments to Drugs: MD Applications in Drug Design. *Molecules* **23**, 3269 (2018).
79. Hornak, V., Okur, A., Rizzo, R. C. & Simmerling, C. HIV-1 protease flaps spontaneously open and reclose in molecular dynamics simulations. *Proceedings of the National Academy of Sciences* **103**, 915–920 (2006).
80. Umezawa, K. & Kii, I. Druggable Transient Pockets in Protein Kinases. *Molecules* **26**, 651 (2021).
81. Ghosh, R., Chakraborty, A., Biswas, A. & Chowdhuri, S. Identification of polyphenols from *Broussonetia papyrifera* as SARS CoV-2 main protease inhibitors using *in silico* docking and molecular dynamics simulation approaches. *J Biomol Struct Dyn* **39**, 6747–6760 (2021).
82. Fischer, A., Smieško, M., Sellner, M. & Lill, M. A. Decision Making in Structure-Based Drug Discovery: Visual Inspection of Docking Results. *J Med Chem* **64**, 2489–2500 (2021).
83. He, J. *et al.* Identification of selective *mtb* DHFR inhibitors by virtual screening and experimental

approaches. *Chem Biol Drug Des* **100**, 1005–1016 (2022).
84. Gentile, D. *et al.* An Integrated Pharmacophore/Docking/3D-QSAR Approach to Screening a Large Library of Products in Search of Future Botulinum Neurotoxin A Inhibitors. *Int J Mol Sci* **21**, 9470 (2020).
85. Irsal, R. A. P., Gholam, G. M., Dwicesaria, M. A., Mansyah, T. F. & Chairunisa, F. Exploring the potential of Scabiosa columbaria in Alzheimer's disease treatment: An in silico approach. *J Taibah Univ Med Sci* **19**, 947–960 (2024).
86. Irsal, R. A. P., Gholam, G. M., Dwicesaria, M. A. & Chairunisa, F. Computational investigation of Y. aloifolia variegate as anti-Human Immunodeficiency Virus (HIV) targeting HIV-1 protease: A multiscale in-silico exploration. *Pharmacological Research - Modern Chinese Medicine* **11**, 100451 (2024).

Supplementary Files

This is a list of supplementary files associated with this preprint. Click to download.

- SupportingMaterial.zip